ELSEVIER

Journal of Quantitative Spectroscopy & Radiative Transfer 105 (2007) 326–355

Journal of Quantitative Spectroscopy & Radiative Transfer

www.elsevier.com/locate/jqsrt

Fourier transform measurements of water vapor line parameters in the 4200–6600 cm^{-1} region

Alain Jenouvrier[a,*], Ludovic Daumont[a], Laurence Régalia-Jarlot[a], Vladimir G. Tyuterev[a], Michel Carleer[b], Ann Carine Vandaele[c], Semen Mikhailenko[d], Sophie Fally[b]

[a]*Groupe de Spectrométrie Moléculaire et Atmosphérique, UMR CNRS 6089, UFR Sciences, Moulin de la Housse, B.P. 1039, 51067 Reims Cedex 2, France*

[b]*Service de Chimie Quantique et de Photophysique ,CP 160/09, Université Libre de Bruxelles, 50 Av. F.D. Roosevelt, B-1050 Brussels, Belgium*

[c]*Institut d' Aéronomie Spatiale de Belgique, Av. Circulaire 3, B-1180 Brussels, Belgium*

[d]*Laboratory of Theoretical Spectroscopy, Institute of Atmospheric Optics, Russian Academy of Sciences, 1, Av. Akademichesskii, 634055 Tomsk, Russia*

Received 11 July 2006; received in revised form 3 November 2006; accepted 8 November 2006

Abstract

New high-resolution water vapor absorption spectra were obtained at room temperature in the 4200–6600 cm^{-1} spectral region by combining Fourier transform spectrometers (FTS) with single and multiple reflection cells. With absorption paths from 0.3 to 1800 m in pure and air diluted water vapor, accurate measurements of about 10400 lines in an intensity range from 10^{-29} to 10^{-19} cm/molecule have been performed. Positions, intensities, self- and air-broadening coefficients and air-induced shifts were determined for the $H_2^{16}O$, $H_2^{17}O$, $H_2^{18}O$ and HDO isotopologues. The rovibrational assignment of the observed lines was performed with the use of global variational predictions and allowed the identification of several new energy levels. One major contribution of this work consists of the identification of 3280 new weak lines. A very close agreement between the new measured parameters and those listed in the database is reported as well as between the observations and the most recent variational calculations for the positions and the intensities. The present parameters provide an extended and homogeneous data set for water vapor, which is shown to significantly improve the databases for atmospheric applications, especially in the transmission windows on both sides of the band centered at 5400 cm^{-1}.

Keywords: Water vapor; Line intensity; Broadening; Atmospheric absorption; Fourier transform spectroscopy

1. Introduction

Through its absorption from the infrared to the ultra violet region, the water vapor, which is the main atmospheric absorber, plays an important role in the radiation budget of the Earth's atmosphere. In spite of

*Corresponding author. Tel./fax: +33 3 26 91 33 33.
E-mail address: alain.jenouvrier@univ-reims.fr (A. Jenouvrier).

0022-4073/$ - see front matter © 2006 Elsevier Ltd. All rights reserved.
doi:10.1016/j.jqsrt.2006.11.007

extensive experimental measurements from the (near) infrared to the ultraviolet regions and of recent advances in the theoretical modeling of the absorption spectrum (see [1] and references therein), the discrepancy between the calculated averaged absorption based on known spectroscopic data and the measured ones remains an open question. In earlier papers [2–4], the 9250–26,000 cm^{-1} spectral region was investigated by the Brussels–Reims group. The measurements were obtained by combining high-resolution Fourier spectroscopy with a long-path absorption cell allowing the characterization of very weak, previously unobserved, lines. The contribution of these lines to the absorption spectrum remains very weak and is not expected to solve the problem. Since then, recent assignments [5] of most of the lines, by a theoretical analysis using variational calculations, lead to the identification of transitions involving more than 150 vibrational exited states of $H_2^{16}O$.

Another aspect to be considered is the detailed characterization of the very weak absorption due to H_2O lines in the so-called atmospheric transparent windows. These regions are usually chosen for astronomical observations and trace species detection where interferences between the absorption lines of water and those of the target trace species are of first interest.

In the continuity of our previous work, and going towards the infrared, the present paper investigates the 4200–6600 cm^{-1} spectral range, which covers the 4200–5000 cm^{-1} and 5700–6600 cm^{-1} transparency windows.

The water spectrum in this region has already been the subject of numerous studies (see for example [6–22] for $H_2^{16}O$, [15,21,23–28] for $H_2^{18}O$, [15,21–23,28,29] for $H_2^{17}O$, and [21,30–33] for HDO). The absorption of isotopically enriched samples has recently been investigated by cw-CRDS technique [21] in the 6130–6750 cm^{-1} spectral region. Previous studies of water spectra between 500 and 8000 cm^{-1} were summarized by Toth in two papers [22,34]. The line parameters of the 7579 rotation-vibration transitions in the 4200–6600 cm^{-1} region from this compilation are included in the most recent version of the HITRAN database [35], where the line strengths have been corrected, in some cases, by as much as 20% when compared with the earlier HITRAN 2000 [36], especially for the region above 5750 cm^{-1}.

The present paper describes a new set of experimental line parameters in the 4200–6600 cm^{-1} spectral region, which complements our previously published line lists [2–4] in the 9250–26,000 cm^{-1} spectral range. Those were determined in similar conditions of pressure, temperature, and air dilution with the same technique of Fourier transform spectroscopy. Special attention was paid to the characterization of weak absorption lines by the use of long absorption path-lengths and, consequently, extended information on observed energy levels for some upper vibrational states was obtained.

The primary aim of this work is the accurate characterization of the line intensities, in particular for weak lines, and of the line broadenings.

After a brief description of the experimental set-up and the data analysis in Section 2, the results including all the line parameters will be discussed with regard to the most recent experimental data and calculations in Section 3.

2. Experimental conditions

In the 4200–6600 cm^{-1} spectral region, the intensities of the lines measured in this work cover a large dynamic range of 10 decades (10^{-29}–10^{-19} cm/molecule) so that reliable measurements must be performed under various experimental conditions. The very weak lines are only observed in long-path absorption spectra while the most intense lines need shorter paths. Three experimental set-ups, using long, medium and short path-lengths (Table 1) were, therefore, chosen in order to cover the wide intensity range.

The experimental set-up for long path absorption spectra has already been presented in detail elsewhere [37]. It will only be briefly described in the present work. Spectra were recorded at high-resolution with a Bruker IFS 120M FTS (thereafter called ULB/IASB FTS) coupled to a multiple-reflection absorption cell having a 50 m base length. The unapodized resolution (0.015 cm^{-1}, which corresponds to 60 cm of MOPD in the Bruker definition) is lower than or close to the full width of the lines in our experimental conditions.

The cell was set with Al + MgF_2-coated mirrors and CaF_2 windows. A 250 W tungsten halogen lamp (ORIEL) was used as the light source in combination with different optical filters. An InSb detector, operating at liquid nitrogen temperature and sensitive over the whole spectral range investigated, was used. The co-addition of 1024 interferograms, leading to a total recording time of 15 h, proved to be adequate to obtain a root mean square (RMS) signal-to-noise (S/N) ratio (expressed as the maximum signal amplitude divided by

Table 1
Summary of laboratory measurement conditions for FT spectra of water vapor in the 4200–6600 cm^{-1} spectral range

Region (cm^{-1})	Path length (m)	H_2O pressure (hPa)	Air pressure (hPa)	Temperature (K)	Run
Long path cell + ULB/IASB FTS (*Resolution* = 0.015 cm^{-1})					
2400–7200[a]	3.6	12.26	1013	296	*a*
4600–7200	201.84	13.17	0	293	*b*
2400–5000	201.84	13.17	0	293	*c*
4600–7200	602.32	13.17	0	294	*d*
4600–7200	602.32	15.33	169.7	293	*e*
4600–7200	602.32	15.33	340.7	293	*f*
2400–5000	602.32	13.24	0	293	*g*
2400–5000	602.32	4.04	0	293	*h*
2400–5000	602.32	4.04	166.9	293	*i*
2400–5000	602.32	4.04	333.6	293	*j*
4600–7200	1203.04	13.17	0	294	*k*
2400–5000	1203.04	13.34	0	293	*l*
4600–7200	1803.76	19.30	0	293	*m*
Medium path cell + GSMA FTS (*Resolution*: 0.010 cm^{-1})					
3950–7900	2.17	2.73	0	295	*n*
3950–7900	32.17	5.60	0	295	*o*
3950–7900	32.17	11.40	0	295	*p*
3950–7900	32.17	22.66	0	295	*q*
Short cell + GSMA FTS (*Resolution*: 0.007 cm^{-1})					
3950–7900	0.30	1.35	0	296	*r*
3950–7900	0.30	2.73	0	296	*s*
3950–7900	0.30	6.80	0	296	*t*
3950–7900	0.30	12.62	0	296	*u*
3950–7900	0.30	19.74	0	296	*v*

[a]This spectrum was recorded with the cell fully evacuated. The H_2O and air pressures given are for the 3.6 m path-length in ambient air outside the cell.

twice the RMS noise amplitude) of about 5000 and 1600 for the runs *b* and *m* with paths of 202 and 1804 m, respectively (Table 1). These high S/N ratios are a necessary condition for the observation of the very weak absorption lines. All the spectra were recorded at room temperature (293 K ± 2 K), which was monitored in the cell by three platinum-resistance thermometers placed on the walls of the cell at its center and its two ends. The temperature along the cell is not stabilized, so that differences between the two ends of the cell, of the order of 2 K, can be sometimes observed. The atmospheric water absorption occurring along the path between the cell and the spectrometer has been recorded (run *a*), and was carefully removed, as described earlier [38]. This procedure has been applied to the spectra recorded with 202 and 602 m of absorption path-lengths where the external contribution to the absorption spectra, strongly depending on the humidity within the room, was significant. The correction was considered to be negligible for longer paths (<0.5%). The pressure was measured with a MKS Baratron capacitance manometer.

The medium (runs *n–q*) and short (runs *r–v*) path absorption spectra have been obtained with the homemade step-by-step FTS of the Reims group (thereafter denoted as GSMA FTS) coupled either to a 1 m long multiple-reflection cell or to a 0.3 m long single path cell. Unapodized resolutions of 0.01 and 0.007 cm^{-1} (MOPD = 50 and 74 cm) were used for the 32 and 0.30 m of path spectra. S/N ratios were over 850, which is sufficient to accurately describe the intense lines. In both cases, the path between the cells and the spectrometer as well as the instrument itself has been pumped down to a residual pressure of 10^{-2} hPa. Small narrow features observed at the top of the strongest lines were easily accounted for in the data reduction. H_2O pressures in the range 1.3–22.7 hPa were used with the two cells and the temperature was accurately stabilized.

The natural water vapor samples were prepared from tri-distilled and carefully degassed liquid water. In order to avoid condensation on the inner mirrors and on the cell windows and walls, the partial pressures were

selected to be well below the saturated vapor pressure. The spectra of water in air mixtures were obtained by introducing progressively air (Air Liquide, $H_2O < 5$ ppm) into the cell already filled with water vapor (runs *e*, *f*, *i*, *j*). For both pure and diluted samples, a period of several hours was waited after the filling of the cell for pressure and temperature stabilization as well as dilution homogenization, which was constantly monitored through the observation of the intensity of the output signal. If no change indicating any problem such as condensation or variation of the partial pressure was observed, the spectra were recorded.

Fig. 1 presents an overview of the absorption spectrum recorded with a path-length of 1203 m and a pressure of 13.2 hPa of pure water. It also shows selected regions where the four species $H_2^{16}O$, $H_2^{17}O$, $H_2^{18}O$ and HDO are observed.

Despite a careful degassing of the liquid water before introduction into the cell, some absorption features of CO_2 and NH_3 with absorption depths lower than 0.01 have been detected in the longest paths' spectra. They were identified using the parameters given in the HITRAN compilation [35] for CO_2. The abundance was found to be of about 0.01% of the total sample pressure. The presence of NH_3 is much more surprising and can be ascribed to the fact that this polar molecule is not removed in the distillation process. Very little information is given in the literature on the NH_3 line positions and strengths. Assignments of the most intense lines have been made from [35] in the spectral region up to 5300 cm^{-1} and from [21,39] in the spectral region above 6130 cm^{-1}. The residual concentration, which is not due to some prior sample in the cell, has been evaluated from [35] to be about 2.5×10^{-4}% of the total sample pressure. Note that these NH_3 lines have also been observed elsewhere in an earlier work [21].

Abnormally high HDO intensities have been observed in the long path absorption spectra (i.e. 200–1800 m), indicating enhanced HDO concentrations compared to natural water. The phenomenon can be explained by the study of the HDO and D_2O spectra in the near infrared and visible regions performed 3 years ago. Since this time, traces of HDO have remained on the walls of the cell and could not be entirely eliminated even after continuous pumping and several dilutions in natural water. The HDO concentration, which varies for each run after the pumping and the filling of the cell, has then been calculated in every spectrum from characteristic selected lines in order to ensure the reproducibility of the observed respective intensities.

3. Data analysis

The line parameters (positions, line areas and line widths) of $H_2^{16}O$, $H_2^{17}O$, $H_2^{18}O$ and HDO were derived by a non-linear least squares fitting procedure. Three different programs: WSPECTRA [40], BFIT [41] and MULTIFIT [42] were used to fit the lines depending on the type of spectrometer and the density of the lines in a given region. The first one, which runs directly from the Bruker output format, fits the observed lines one-by-one to the exponential of a theoretical profile (Voigt in this case) convolved by the instrumental function as described in our previous study [2]. The second one, operating in the same way, is meant for more restricted and congested regions. The third one, which utilizes a multifit procedure, was generally used for the spectra recorded by the GSMA FTS at a given path-length and different sample pressures. An intercomparison has been made on selected lines of a given spectrum to check the reproducibility of the parameters (position, intensity, broadening) fitted with the three programs, which was better than 0.5%. A similar comparison between the spectra recorded with the two spectrometers leads to a similar agreement in position ($d\nu < 0.0005$ cm^{-1}), intensity ($dI < 0.5\%$) and self-broadening ($d\gamma < 1\%$) on average. Therefore, the parameter values given hereafter are averages of all individual values retrieved from spectra recorded by one of the two instruments, using one of the three software codes.

The line positions were obtained from a subset of six pure water vapor spectra recorded with the ULB/IASB FTS at the same $H_2^{16}O$ partial pressure of around 13 hPa (runs *b*, *c*, *d*, *g*, *k*, *l* in Table 1). Calibrated line positions expressed as vacuum wavenumbers were obtained by comparing the positions of well-defined and isolated lines of $H_2^{16}O$ and additional HDO lines belonging to the six above-mentioned spectra to the HITRAN positions [35]. In such a way, a fitted curve $\nu(\mathrm{ref})_{\mathrm{vacuum}}-\nu(\mathrm{obs})_{\mathrm{air}} = 4.0975 \times 10^{-3} + 3.7 \times 10^{-6}\nu$ was calculated and this correction curve was then applied to all the line positions. Of course in doing so, because we compared line positions recorded at a certain H_2O pressure to table values given at zero pressure, the corresponding water self shift is included in the correction curve. One has to notice that the spectra recorded at 4.04 and 19.30 hPa (runs *h*, *i*, *j* and *m*) were excluded from the lines position determination because the

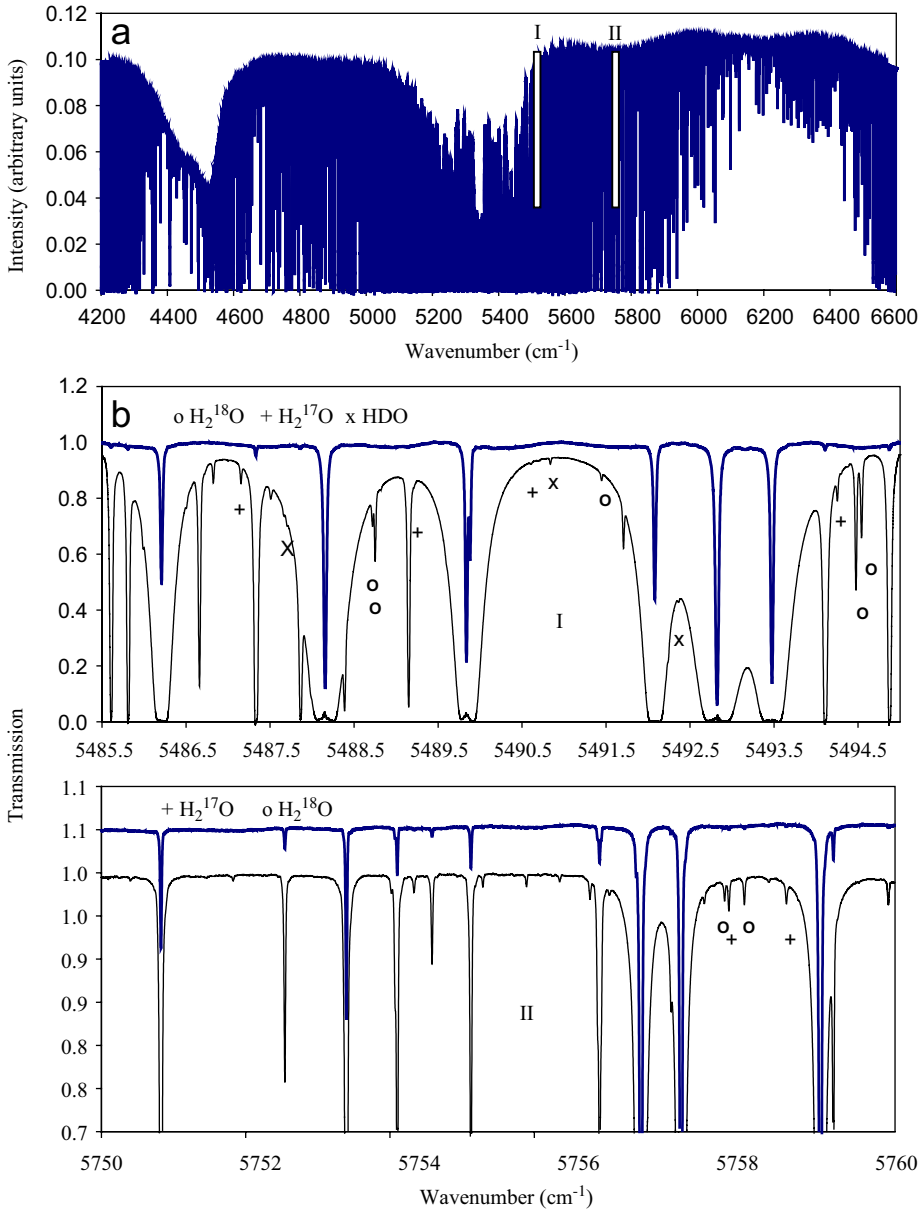

Fig. 1. (a) Overview of the pure water absorption spectrum between 4200 and 6600 cm^{-1} obtained at room temperature with an absorption path of 1203 m and 13 hPa of water (runs *k* and *l*). (b) Detailed views of the pure water transmission spectra near the band center showing the absorption features of the different isotopologues $H_2^{16}O$, $H_2^{18}O$, $H_2^{17}O$ and HDO: I—The upper and lower traces correspond to spectra obtained, respectively, with a path of 0.3 m and a pressure of 19.7 hPa (run *v*) and with 202 m and 13.2 hPa (run *b*). II—The upper and lower traces correspond to spectra obtained with a path of 202 m and a pressure of 13.2 hPa (run *b*) and with 1804 m and 19.3 hPa (run *m*).

self-shift correction is obviously wrong by a value higher than the precision of the wavenumber measurements. Also, spectra recorded with the fully evacuated GSMA FTS were used only to measure intensity and self-broadening of the most intense lines. At the final stage of the calibration procedure, considering all the lines, the line positions agree with those of Toth [22] and HITRAN [35] to better than 0.0002 cm^{-1} on average, which is of the order of the experimental uncertainty.

The line areas (A_σ in cm^{-1}) are converted into conventional line-integrated strengths (or intensities) S_σ expressed in cm/molecule by the relationship:

$$S_\sigma = A_\sigma \frac{P_0 T}{n_L T_0 P l}, \tag{1}$$

where T (in K) and P (in atm) are the temperature and pressure in the cell, $T_0 = 273.15\,K$, $P_0 = 1$ atm, l (in cm) is the absorption path-length and $n_L = 2.6868 \times 10^{19}$ molecule/cm^3 is the Loschmidt number.

The final intensity dataset has been constructed by merging the different experiments with the restrictive condition: peak absorptions higher than 80% were rejected. At the chosen resolution, it corresponds approximately to intensities of 5×10^{-23}, 6×10^{-24}, 2.5×10^{-24}, 8×10^{-25} and 6×10^{-25} cm/molecule in the spectra recorded with respective absorption paths of 32, 200, 600, 1200, and 1800 m. One has to mention that spectrum m (1800 m) was only used to measure intensities of very weak lines.

The self- and air-broadening parameters (γ_{self} and γ_{air}) and air frequency shifts (δ_{air}), expressed in (cm^{-1}/atm) are related to the partial H_2O and air pressures (in atm) in the cell by the usual linear expressions:

$$\Gamma/2 = \left(\gamma_{H_2O} \times P_{H_2O}\right) + \left(\gamma_{air} \times P_{air}\right), \tag{2}$$

$$\nu_{buffer} = \nu_0 + \delta_{H_2O} \times P_{H_2O} + \delta_{air} \times P_{air}, \tag{3}$$

where ν_0 (in cm^{-1}) is the "zero" pressure line position and Γ (in cm^{-1}) is the full-width at half-maximum of the Lorentzian component.

The self-broadening parameters (γ_{H_2O}) were logically determined from the subset of pure water vapor spectra (runs b, c, d, g, h, k, l, m and n–v in Table 1), rejecting outliers such as saturated lines, as it was done for the determination of the lines position. The air-induced shift parameters have been obtained from Eq. (3) by analyzing the spectra of H_2O/air mixtures with identical H_2O partial pressures (runs h, i, j in Table 1) or close to each other H_2O partial pressures (runs d, e, f in Table 1), so that the self-contribution could be considered equal. In the latter case, the H_2O pressure difference of about 2 hPa between run d and runs e, f induces an error on the air-induced pressure shifts estimated to be of the order of 3×10^{-4} cm^{-1}/atm when considering the mean values of the self-induced shifts parameters reported by Toth [43] or Grossmann [44] in the ν_2 band and near 13500 cm^{-1}, respectively. This value remains lower than the experimental uncertainties and can, therefore, be neglected. The same statement applies to the air-broadening parameters. An additional recording of the atmospheric water absorption outside the cell (run a) was used to determine the air-broadening effects on the strongest lines. The air-broadening and air-induced shift parameters (γ_{air} and δ_{air}) have accordingly been obtained from Eqs. (2) and (3), respectively, in which the P_{H_2O} term was kept constant and thus canceling by subtraction within each set of three spectra. No attempt was made to determine the self-shifts.

The air-induced shift parameters have been obtained from Eq. (3) using spectra with the same H_2O partial (runs h, i, j) or close enough H_2O partial pressures (runs d, e, f), so that the self-shifts can be considered identical. In the latter case, the difference in H_2O pressure of about 2 hPa induces an uncertainty on the air-induced pressure shifts estimated to be of the order of 3×10^{-4} cm^{-1}/atm when considering the mean values of the self-induced shifts parameters reported by Toth [43] or Grossmann [44] in the ν_2 band and near 13,500 cm^{-1}, respectively. This value remains lower than the experimental uncertainties and can therefore be neglected.

For the comparison with the literature and the databases, the line parameters measured here near 293 K (T_1) have been converted to the temperature T_2 of 296 K (as in HITRAN), by using the following approximate relations:

$$S_\sigma(T_2) = S_\sigma(T_1)\left(\frac{T_1}{T_2}\right)^{3/2} e^{-E''(hc/k)\left((1/T_2)-(1/T_1)\right)}, \tag{4}$$

$$\gamma(T_2) = \left(\frac{T_1}{T_2}\right)^{n} \gamma(T_1), \tag{5}$$

where E'' is the lower state energy of the transition in cm^{-1}, n is the line width temperature dependence parameter, assumed here to be equal to that used in the HITRAN database ($n = 0.6$) for the air broadening.

Even if this value may not be constant for all transitions, its influence remains very small on the retrieved parameters when the temperature difference is only 3° K.

The possible sources of experimental errors, both systematic and statistical, on the derived parameters can be identified as following:

(a) Systematic errors arising from the uncertainties on the pressure (1%), the temperature (1%) and the path-length (0.5%) and affecting all the lines in the same way.
(b) Statistical uncertainties resulting from the fitting procedures (fitting programs and regression analysis), which differ from line to line. These are generally larger for weak or blended lines than for the strong and well-isolated lines. In the present work, only lines for which the maximum of absorption is lower than 80% in the given experimental conditions have been taken into account to avoid possible saturation effects. When the lines were observed in several water spectra, the parameters were obtained by calculating the average value of the individual ones and the resulting RMS deviation is used as the uncertainty, implicitly including, in principle, the constant contributions on pressure, temperature and path-length. If not, as it is often the case for very weak lines only observed with long paths, the 3σ uncertainty resulting from the fit was used as the statistical uncertainty.

The complete list of the fitted parameters for the observed lines at 293 K and its accompanying readme file are available either on the Web site of the Service de Chimie Quantique et Photophysique (http://www.ulb.ac.be/cpm) or upon request to the authors. This list contains all the observed lines of the four H_2O isotopologues and is composed of their parameters with the associated statistical uncertainties, the rotational and vibrational assignments and the lower state energies. The lines overlapped by NH_3, CO_2 or by an unidentified component are clearly indicated. Another line list containing intensities converted at 296 K and excluding unassigned lines is also available on request. In these line lists, when the line fitting procedure resulted in a Lorentzian width higher than its associated 3σ uncertainty, as it occurs for very weak and blended lines, the self- and air-broadening parameters are not provided. The uncertainties on the parameters must be considered as the sum of statistical (quoted into the lists) and systematic (~3%) uncertainties.

4. Results and discussion

4.1. Line identifications, positions and assignments

About 10,400 lines have been measured in the 4200–6600 cm^{-1} spectral range. Among them, 9494 observed lines could be assigned (10,161 assigned transitions, taking into account an overlapping of some of the resulting lines) to the 4 major isotopic water species. A statistic of the lines is given in Table 2 where the number of

Table 2
Statistics of the lines in the 4200–6600 cm^{-1} spectral range: comparison of the number of lines observed in this work for the isotopologues of the water vapor with the most complete literature data

		This work	HITRAN 2004 [35]	Toth [22]	Mikhailenko et al. [19]	Macko et al. [21][a]
Nbr of lines		10,394				3526
Unassigned		128				
Impurities	NH_3	511				
	CO_2	271				
Nbr of assignments	$H_2^{16}O$	5438	4069	3543	3394	1499
	$H_2^{18}O$	1060	1127	617	590	220
	$H_2^{17}O$	576	684	312	271	82
	HDO	3087	1699	1801	848	1368
	Total	10,161	7916	6273	5101	3169

[a]The data of Macko et al. [21] are restricted to the 6130–6600 cm^{-1} spectral range.

Table 3
Statistics of the lines in the 4200–6600 cm^{-1} spectral range: number of assignments per band with their upper and lower J quantum numbers

Bands	$H_2^{16}O$	J''_{min}, J''_{max}	$H_2^{17}O$	J''_{min}, J''_{max}	$H_2^{18}O$	J''_{min}, J''_{max}	$HD^{16}O$	J''_{min}, J''_{max}
001–000	249	4, 17	19	7, 12	43	6, 13		
002–000	6	10, 13						
002–010	88	0, 8						
011–000	1349	0, 20	368	1, 9	537	0, 15	840	0, 18
011–010	30	6, 12						
020–000	32	7, 15						
021–000	174	4, 19	5	7, 12	27	5, 14	340	0, 13
021–010	433	0, 15	7	1, 8	31	1, 8	40	1, 9
030–000	713	0, 16	30	1, 10	98	0, 13	243	1, 16
031–010	51	4, 13					14	1, 7
031–020	18	1, 7						
040–000	395	0, 16	2	3, 8	23	1, 9	50	2, 11
040–010	67	1, 11						
041–020	1	6						
050–000							11	7, 12
050–010	17	3, 10						
100–000	89	5, 18	1	8	5	8, 12		
101–000	63	7, 15					709	0, 17
101–010	80	0, 9					6	0, 1
110–000	1030	0, 17	129	1, 9	258	0, 12	295	1, 16
110–010	3	11						
120–000	168	3, 17	14	5, 10	34	4, 12	138	1, 12
120–010	174	1, 11	1	4	3	1, 2	6	0, 2
130–000							1	0
130–010	53	6, 12						
130–020	1	20						
200–000	49	8, 15			1	9	362	0, 16
200–010	105	0, 10						
210–000							44	4, 14
210–010							4	2, 5

assignments is compared to the most complete observations in this region [19,21,22] and to the HITRAN database [35]. It is seen that a progress compared to HITRAN has been mainly achieved for $H_2^{16}O$ and HDO. These 10161 water transitions are shown band by band in Table 3. Among them, 5438 transitions (5152 lines) were assigned to 26 bands of the $H_2^{16}O$ and correspond to 16 upper vibrational states. About 1060 transitions (1008 lines) were assigned to 10 bands of the $H_2^{18}O$ and correspond to 8 upper vibrational states. For $H_2^{17}O$ 576 transitions (544 lines) were assigned to 10 bands and correspond to 8 upper vibrational states. For HDO, 3087 transitions (2780 lines) were assigned to 19 bands and correspond to 12 upper vibrational states.

Rovibrational assignment of water lines is based on experimental energy levels known from previous studies and on global variational predictions of line positions and intensities [45,46]. The validation of the assignments and the determination of the experimental energy levels and their uncertainties for all four species were performed by using the RITZ program [47], which was successfully applied in previous studies of water spectra [19,21,48]. The observed ground state energy levels from [45] used to calculate the new upper state levels are given in Appendix A. Compared to these studies, more than 4200 transitions included in energy levels determination are due to our new measurements and analysis. This has allowed to significantly improve the accuracy of the experimental energy determination for a large set of rovibrational levels and to add some newly determined levels as described below.

4.1.1. $H_2^{16}O$

Experimental rotation–vibration energy levels from Refs. [18,19,21,49,50] were used to assign lines to the $H_2^{16}O$ species. Practically, for all the levels obtained from assigned transitions, the energy levels are in very

good agreement with previous studies. Though a number of new lines were observed in this work, only one new energy level of the (0 5 0) vibrational state for $J = 4$, $K_a = 0$, $K_c = 4$ was found at 7770.4105 cm^{-1}. In addition, the value of the $J = 2$, $K_a = 1$, $K_c = 2$ level of the (0 5 0) state has been corrected from 7663.7987 cm^{-1} [47] to 7663.6389 cm^{-1}.

4.1.2. $H_2^{18}O$

For the assignment of the $H_2^{18}O$ lines, the energy levels from several experimental studies were used, namely [26] (for the (0 0 0) and (0 1 0) states), [15,28] (for the first triad of vibrational interacting states (0 2 0), (1 0 0), and (0 0 1)), [25,51] (for the second triad of vibrational interacting states (0 3 0), (1 1 0), and (0 1 1)), and [17,21,27] (for the (0 4 0), (1 2 0), and (0 2 1) states). We were able to find 9 new energy levels of the (0 0 1) and (1 0 0) states. The term values of these levels with their uncertainties and the number of transitions are given in Table 4. The observed line positions and term values of the upper levels are in very good agreement with previous studies.

4.1.3. $H_2^{17}O$

The experimental energy levels from [21,28,29,52,53] were used for the assignment of lines. The identification procedure was obvious for the (1 0 0), (0 0 1), (0 4 0), (1 2 0), and (0 2 1) upper states: the lines of six bands corresponding to these upper states could be assigned by comparing observed lines positions to those calculated from experimental energy levels. The assignment of the $3\nu_2$, $\nu_1 + \nu_2$ and $\nu_2 + \nu_3$ bands was more complicated because of the less known rotational structure of the (1 1 0) and (0 1 1) states and previously unknown (0 3 0) state. Using global variational predictions (available at http://spectra.iao.ru) generated with the potential function [43] and dipole moment function [44] of Partridge and Schwenke (hereafter referred as PS) and on the results of the $\nu_2 + \nu_3$ band analysis from [23,29], 470 lines have been assigned to these three bands. Among them, 28 lines belonging to the $3\nu_2$ band ($J_{max} = 9$ and $K_{a\ max} = 5$) were assigned for the first time, 113 lines belong to the $\nu_1 + \nu_2$ band ($J_{max} = 10$ and $K_{a\ max} = 6$) and 329 lines belong to the $\nu_2 + \nu_3$ band with the maximal values ($J_{max} = 15$ and $K_{a\ max} = 8$). The discrepancies between observed and predicted (PS) line positions are plotted on Fig. 2, showing a smooth variation versus wave number without strong outliers. A similar behavior was previously observed for the second triad bands of $H_2^{16}O$ [19] and $H_2^{18}O$ [49] molecules, that tend to ascertain the present assignments.

Our newly assigned line positions as well as data from Refs. [15,21–23,28,29] were simultaneously used to obtain a new set of rotational energy levels for all upper and lower vibrational states involved in these transitions. A very good agreement of the line positions and the rotational energy levels with previous studies [21,23,28,51] was observed for the upper (0 0 1), (1 0 0), (0 4 0), (0 2 1), and (1 2 0) states.

Table 4
New energy levels of the $H_2^{18}O$ molecule: $v_1v_2v_3$ J K_a K_c are the vibration and rotation quantum numbers; E^{obs} are the experimentally determined rovibrational term values (cm^{-1}), δE their corresponding uncertainties (in 10^{-4} cm^{-1}) and N the number of transitions used for determination of each energy level

$v_1v_2v_3$	J	K_a	K_c	E^{obs}	δE	N
1 0 0	12	2	10	5566.2328	5	1
1 0 0	12	3	10	5569.3100	5	1
1 0 0	13	2	11	5846.1453	5	1
1 0 0	13	3	10	6013.4982	5	1
0 0 1	9	9	1	5858.6497	3	2
0 0 1	9	9	0	5858.6497	6	*
0 0 1	11	8	4	6167.6238	2	3
0 0 1	14	4	10	6573.8673	5	1
0 0 1	14	7	7	6920.3125	5	1

Transition to the levels indicated by * is not resolved. The energy for such level was fixed to those of the observed coincident partner and the uncertainty values account for the estimated energy splitting.

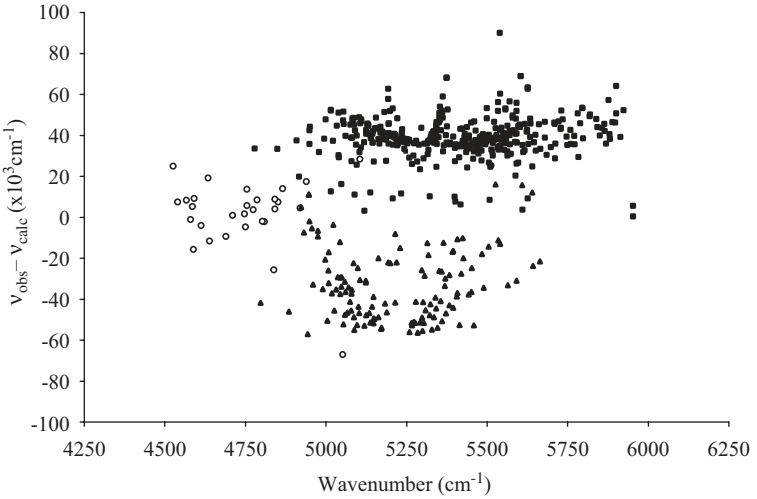

Fig. 2. Comparison between observed and calculated line positions of the $H_2^{17}O$ molecule for the (0 3 0) state (open circles), the (1 1 0) state (full triangles) and the (0 1 1) state (full squares). The calculated values refer to the calculation using the potential energy surface and the pure *ab initio* dipole moment surfaces of Partridge and Schwenke [46].

For the (0 3 0), (1 1 0), and (0 1 1) interacting vibrational states, a new set of 251 rovibrational energies has been obtained, among which 53 levels were experimentally determined for the first time (Table 5). For the set of levels of the (1 1 0) and (0 1 1) states common to previous determinations, our values are generally very close to those reported by Toth [22], except for 4 levels of the (0 1 1) state ($8_{8\ 1}$, $8_{8\ 0}$, $11_{3\ 8}$, and $14_{1\ 14}$) and two levels of the (1 1 0) state ($6_{6\ 1}$ and $6_{6\ 0}$) where a difference amounting up to 1.27 cm^{-1} was observed for $8_{8\ 1}$ and $8_{8\ 0}$ levels of the (0 1 1) state.

The new set of experimental energies of the (0 3 0), (1 1 0), and (0 1 1) states was fitted using a rovibrational Hamiltonian for a triad of interacting states [54]. Similarly to recent works on the second triads of others water isotopic species [19,51] we used the generating function model (G-function) [55,56] for an effective Hamiltonian that takes into account resonance interactions of both anharmonic and Coriolis type. The results of the fit of the energy levels for all three states are shown in Table 6. The standard deviation between experimental and calculated values is about 0.008 cm^{-1} for the 251 fitted energy levels. Among them, 207 levels are fitted with discrepancies $dE = |E^{obs}–E^{calc}|$ lower than 0.008 cm^{-1} and only three levels are fitted with dE bigger than 0.02 cm^{-1}: −0.0306 cm^{-1} for $1_{0\ 1}$ of the (0 3 0), +0.0218 cm^{-1} for $7_{4\ 3}$ and −0.0242 cm^{-1} for $8_{5\ 3}$ of the (1 1 0). The largest discrepancies between values previously determined by Toth ([22], http://mark4sun.jpl.nasa.gov) and our observations and calculations for 12 levels of the (0 1 1) and (1 1 0) states are given in Table 7.

4.1.4. HDO

As for the three previous species, available experimental energy levels were used for the assignment of the HDO lines. We were able to assign the transitions of 17 bands corresponding to 12 upper vibrational states. The energy levels deduced from our study are generally in very good agreement with the energy levels of Refs. [21,30–33,57]. Seventy-one new rotational energy levels of the (0 1 1), (0 4 0), (1 1 0), (1 2 0), and (2 0 0) states are listed in Table 8. Note that, due to the very strong coupling of the rotational energy levels of the (0 4 0) and (1 2 0) states, the vibrational assignment of some levels (for example, $K_a = 3$ and 4 ($J = 3$, 4, 5, and 7) and $K_a = 2$ ($J = 10$ and 11) of the (0 4 0) state in Table 7) is ambiguous. It is well known that in such cases, a string of quantum numbers should be taken as a "nominative labeling" rather than a firm assignment. In this paper we have chosen to follow vibrational labeling of Refs. [31,32,58]. Discrepancies between observed and calculated (PS) line positions corresponding to the different upper vibrational states (0 3 0), (1 1 0) and (0 1 1) are shown on Fig. 3 where all the values are lower than 0.12 cm^{-1} increasing our confidence in the assignments.

Table 5
New energy levels of the $H_2^{17}O$ molecule: $v_1v_2v_3$ J K_a K_c are the vibration and rotation quantum numbers; E^{obs} are the experimentally determined rovibrational term values (cm^{-1}), δE their corresponding uncertainties (in $10^{-4}cm^{-1}$) and N is the number of transitions used for determination of each energy level

$v_1v_2v_3$	J	K_a	K_c	E^{obs}	δE	N	$v_1v_2v_3$	J	K_a	K_c	E^{obs}	δE	N
0 1 1	8	8	1	7162.9893	10	*	0 3 0	2	2	1	4844.3875	5	1
0 1 1	8	8	0	7162.9893	5	1	0 3 0	2	2	0	4845.3141	3	2
0 1 1	9	8	2	7382.3954	5	1	0 3 0	3	1	3	4810.5754	5	1
0 1 1	9	8	1	7382.3954	10	*	0 3 0	3	1	2	4846.8369	5	1
0 1 1	10	6	4	7226.4304	3	2	0 3 0	3	2	2	4915.8846	5	1
0 1 1	10	8	3	7625.1452	10	*	0 3 0	3	2	1	4920.3556	3	2
0 1 1	10	8	2	7625.1452	5	1	0 3 0	3	3	0	5053.1729	3	2
0 1 1	11	3	8	7138.6102	5	1	0 3 0	4	1	4	4891.8240	5	1
0 1 1	11	4	7	7223.8621	5	1	0 3 0	4	2	3	5010.3086	5	1
0 1 1	11	5	7	7323.6025	5	1	0 3 0	4	3	2	5150.2875	3	2
0 1 1	11	5	6	7336.6044	5	1	0 3 0	4	4	1	5328.1610	5	1
0 1 1	11	6	6	7491.1171	5	1	0 3 0	5	1	4	5079.7103	3	2
0 1 1	11	6	5	7492.5438	5	1	0 3 0	5	2	3	5153.1108	5	1
0 1 1	11	7	5	7680.8617	5	1	0 3 0	6	1	6	5110.8756	5	1
0 1 1	12	4	9	7450.5117	5	1	0 3 0	6	3	4	5417.1229	5	1
0 1 1	12	5	7	7635.2592	5	1	0 3 0	7	2	6	5423.6826	5	1
0 1 1	12	6	6	7783.1327	5	1	0 3 0	7	5	2	5980.5003	5	1
0 1 1	13	3	10	7736.0149	5	1	0 3 0	9	5	4	6395.4939	3	2
0 1 1	13	4	10	7749.0545	5	1							
0 1 1	14	1	14	7341.5951	5	1	1 1 0	6	6	1	6332.7695	5	1
0 1 1	14	1	13	7620.7840	5	1	1 1 0	6	6	0	6332.7695	10	*
0 1 1	14	2	12	7859.5166	5	1	1 1 0	8	5	4	6520.4487	5	1
0 1 1	15	2	14	7919.2991	5	1	1 1 0	8	5	3	6520.8625	5	1
0 3 0	1	0	1	4680.8719	5	1	1 1 0	9	2	8	6300.3944	5	1
0 3 0	1	1	0	4713.5463	3	2	1 1 0	9	5	5	6737.3837	5	1
0 3 0	2	0	2	4727.4507	5	1	1 1 0	10	4	7	6821.2014	10	1
0 3 0	2	1	2	4748.9481	5	1							

Transitions to the levels indicated by * were not resolved. The energy for such levels was fixed to those of observed coincident partners and the uncertainty values account for an estimated energy splitting.

Table 6
Range of quantum numbers and number of levels for the fit of experimental energy levels of the second triad interacting states of the $H_2^{17}O$ molecule

State	This study		Toth [22]	
	$(J, K_a)_{max}$	Nbr. Lev.	$(J, K_a)_{max}$	Nbr. Lev.
(0 3 0)	9, 5	23		
(1 1 0)	10, 6	78	11, 6	82
(0 1 1)	15, 8	150	15, 8	130
Total		251		212

Finally 128 weak lines, with intensities less than 2.5×10^{-26} cm/molecule remain unassigned, that corresponds to ~1% only of a total number of recorded water vapor lines. The corresponding line list is given in the readme file of the line lists (http://www.ulb.ac.be/cpm).

In total, for all the four water isotopic species we have observed and assigned 3280 new lines which are not present in the HITRAN-2004 or GEISA/IASI-2003 data base compilations [35,59].

Table 7
Experimental and calculated energy levels of the (0 1 1) and (1 1 0) states of the $H_2^{17}O$ molecule: $v_1v_2v_3$ J K_a, K_c are the vibration and rotation quantum numbers; E^{calc} are the calculated rovibrational term values using G-function Hamiltonian fitted parameters (cm^{-1}), E^{obs} the experimentally determined rovibrational term values (cm^{-1}), and dE the discrepancies between experimental and calculated term values (cm^{-1})

$v_1v_2v_3$	J	K_a	K_c	E^{calc}	E^{obs}	dE	E^{obs}	dE
				This work			http://mark4sun.jpl.nasa.gov	
0 1 1	8	8	1	7162.9973	7162.9893	−0.0080	7164.2639	1.2666
0 1 1	8	8	0	7162.9973	7162.9893	−0.0080	7164.2653	1.2680
0 1 1	11	3	8	7138.6083	7138.6102	0.0019	7139.2634	0.6551
0 1 1	14	1	14	7341.5957	7341.5951	−0.0006	7342.5385	0.9428
1 1 0	6	6	1	6332.7707	6332.7695	−0.0012	6333.5990	0.8283
1 1 0	6	6	0	6332.7709	6332.7695	−0.0014	6333.5984	0.8275
1 1 0	7	6	2	6501.9139			6502.6272	0.7133
1 1 0	7	6	1	9501.9165			6502.6293	0.7128
1 1 0	8	2	6	6210.3653			6210.8367	0.4714
1 1 0	8	3	5	6283.6667			6284.1958	0.5291
1 1 0	10	1	9	6508.6054			6509.1574	0.5520
1 1 0	10	3	8	6675.2662			6675.5276	0.2614

4.2. Line intensities

4.2.1. Comparison with experimental data

Line intensities in the range 4×10^{-29}–2.8×10^{-20} cm/molecule were measured in this study, allowing the characterization of the weak absorption lines for the different isotopologues of the natural water vapor, as stated above. For all the observed lines given in the list, the intensities have been measured. In the cases where several assignments correspond to an observed single line, the total intensity of the different components is given.

A general comparison between our new dataset with the most extended experimental data in this spectral range as well as with PS predictions based on an *ab initio* dipole moment function [45,46] is shown in Table 9 where the integrated band intensities (ΣS_σ) for the different isotopologues and the number of corresponding lines are given. Despite the great number of lines in the present data set, the numerous newly measured weak lines provide a relatively small contribution to the integrated intensity, which is in very close agreement when compared to HITRAN [35].

For $H_2^{16}O$, it is seen that the overall absorption in this frequency range is in great part carried by the preponderant (0 1 1)–(0 0 0) band where our number of lines is only slightly higher than those listed in the database. The number of $H_2^{17}O$ and $H_2^{18}O$ observed lines is less than in the database and our integrated intensity is slightly lower. The opposite is seen for HDO where a significant number of new lines have been observed. This new data can be of big importance for the absorption in transparency micro-windows and also for the validation of theoretical models.

The line intensities of this work have further been compared line-by-line with values from the literature in Table 10. Considering each original data set, the intensities and spectral ranges as well as the number of lines in common are indicated for each isotopologue. The comparison was based on two quantities: the mean value of the ratio between the intensities of this work and those of the literature data (R) and the regression coefficient (A) of the plots S_σ(this work) $= A \times S_\sigma$(literature). The values of R are shown in Figs. 4–7 for $H_2^{16}O$, $H_2^{17}O$, $H_2^{18}O$ and HDO, respectively and the mean values are collected in Table 10. From these figures and Table 10, the following conclusions can be drawn.

The comparison with the various data sets for $H_2^{16}O$ is made in different intensity ranges from about 10^{-28} to 3×10^{-20} cm/molecule as reflected in Fig. 4. In each case, an increasing spread is observed towards the lower intensities resulting from the difficulty to obtain accurate values for the weak lines. This is also reflected by comparison of the plots (b), (a) and (c) in this order where, for a given intensity, the absorption path increases allowing a better accuracy. For weak lines, a fewer number of outliers is observed in comparison

Table 8
New energy levels of the HDO molecule: $v_1v_2v_3$ J K_a K_c are the vibration and rotation quantum numbers; E^{obs} are the experimentally determined rovibrational term values (cm^{-1}), δE their corresponding uncertainties (in $10^{-4}\,cm^{-1}$), and N the number of transitions used for the determination of each energy level

$v_1v_2v_3$	J	K_a	K_c	E^{obs}	δE	N	$v_1v_2v_3$	J	K_a	K_c	E^{obs}	δE	N
0 1 1	13	3	11	6636.0651	5	1	0 4 0	11	3	9	6744.9361	5	1
0 1 1	13	5	9	6908.6170	3	2	0 4 0	11	3	8	6779.5233	5	1
0 1 1	13	5	8	6913.1983	3	2	0 4 0	12	1	11	16750.6623	5	1
0 1 1	14	3	12	6843.9421	5	1							
0 1 1	14	3	11	6948.3109	5	1	1 1 0	11	9	3	6421.0464	10	*
0 1 1	16	1	15	7110.6189	5	1	1 1 0	11	9	2	6421.0464	5	1
0 1 1	6	2	15	7110.7326	3	2	1 1 0	17	1	16	6355.0674	5	1
0 1 1	16	3	14	7296.7709	5	1	1 1 0	17	2	16	6355.1990	5	1
0 1 1	17	2	16	7342.4104	5	1							
0 4 0	1	0	1	5435.5766	5	1	1 2 0	0	0	0	5506.1869	5	1
0 4 0	3	3	1	5737.9152	5	1	1 2 0	5	5	1	6191.4489	5	1
0 4 0	3	3	0	5737.9427	5	1	1 2 0	5	5	0	6191.4487	5	1
0 4 0	4	3	2	5865.8876	5	1	1 2 0	6	1	5	5878.1166	5	1
0 4 0	4	3	1	5866.0186	3	2	1 2 0	6	6	1	6483.6508	5	1
0 4 0	5	3	3	5944.6974	3	2	1 2 0	6	6	0	6483.6508	5	1
0 4 0	5	3	2	5945.2046	2	4	1 2 0	7	6	2	6590.4938	5	1
0 4 0	5	4	2	6020.4315	5	1	1 2 0	7	6	1	6590.4938	5	1
0 4 0	5	5	1	6330.5035	2	3	1 2 0	8	5	4	6513.7189	5	1
0 4 0	6	3	4	6039.3440	2	3	1 2 0	8	5	3	6513.7258	5	1
0 4 0	6	3	3	6040.8211	5	1	1 2 0	8	6	3	6712.6487	3	2
0 4 0	6	4	3	6112.9653	5	1	1 2 0	8	6	2	6712.6485	3	2
0 4 0	6	4	2	6113.0267	5	1	1 2 0	9	2	7	6337.7553	5	1
0 4 0	6	5	2	6283.4272	5	1	1 2 0	9	6	4	6850.1329	5	1
0 4 0	6	5	1	6283.4274	5	1	1 2 0	9	6	3	6850.1333	5	1
0 4 0	7	3	5	6079.3200	5	1	1 2 0	10	4	6	6642.7341	5	1
0 4 0	7	5	3	6535.1147	5	1	1 2 0	12	1	12	6566.7713	3	2
0 4 0	7	5	2	6535.1155	5	1	1 2 0	13	0	13	6734.9782	5	1
0 4 0	7	6	2	6786.0296	10	*	1 2 0	13	1	13	6735.1219	5	1
0 4 0	7	6	1	6786.0296	5	1							
0 4 0	8	3	6	6203.2428	5	1	2 0 0	11	7	5	7070.7913	5	1
0 4 0	8	4	4	6345.5152	5	1	2 0 0	11	7	4	7070.7914	5	1
0 4 0	8	6	3	6911.4568	5	1	2 0 0	12	7	6	7248.6011	5	1
0 4 0	9	4	5	6485.8610	5	1	2 0 0	12	7	5	7248.5978	5	1
0 4 0	9	5	5	6802.8304	5	1	2 0 0	13	4	10	6974.8213	5	1
0 4 0	10	2	9	6423.2680	5	1	2 0 0	15	1	14	7117.2042	5	1
0 4 0	11	2	9	6686.5007	5	1							

Transitions to the levels indicated by * were not resolved. The energy for such levels was fixed to those of observed coincident partners and the uncertainty values account for an estimated energy splitting.

with the data of Macko et al. [21] originating from CRDS spectra for which the detection limit is as low as 10^{-29} cm/molecule although their measurements are on average about 25% lower than ours (Fig. 4(c)). The spread of discrepancies in the intensity range 10^{-23}–5×10^{-27} cm/molecule with these data is clearly less than that for other available measurements displayed in Figs. 4(a) and (b). This better consistency could be explained by the fact that both data of [21] and ours correspond to the longest optical path and thus to the highest S/N ratio achieved so far in this intensity interval and should allow a more reliable measurement of very weak lines. The data of [21] are the only available for comparison of measured intensities below 2×10^{-27} cm/molecule. Note, however, that these measurements cover a relatively narrow wavenumber range corresponding to the 1.5 μm transparency window, whereas the observations of the present work contain also other weak lines within the absorption band ranges.

Concerning R and A statistical criteria, a good agreement is obtained on average with the other data sets as R and A values are close to unity (Table 10). As the intercept of the linear regression slope S_σ(this

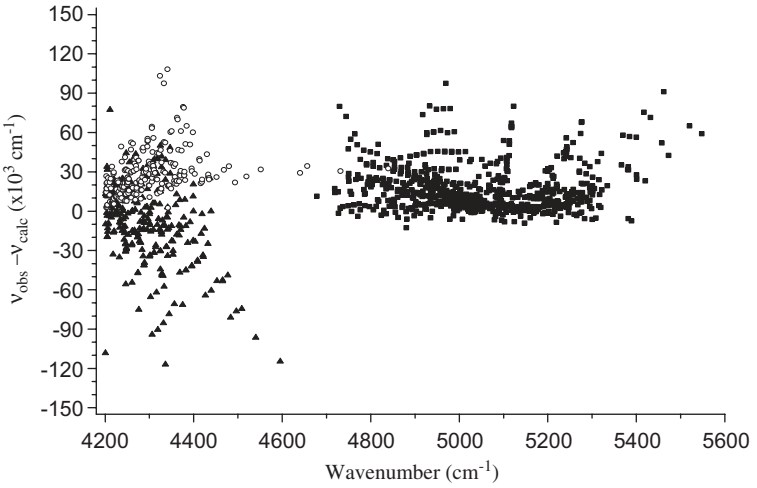

Fig. 3. Comparison between observed and calculated line positions of the HDO molecule for the (0 3 0) state (open circles), the (1 1 0) state (full triangles) and the (0 1 1) state (full squares). The calculated values refer to the calculation using the potential energy surface and the pure *ab initio* dipole moment surfaces of Partridge and Schwenke [46].

work) $= A \times S_\sigma$(literature) is fixed to zero, the value of the A regression coefficient is obviously dominated by contributions of strong and medium lines. Thus the values $A \approx 1$ in Table 10 indicate that intensities of this kind of lines are indeed in a relatively good agreement on average with previous empirical [22,35] and theoretical [43,44] compilations. The value of R corresponds to the median of scatters given in Fig. 4 because positive and negative outliers around the median tend statistically to compensate each others. A value $R = 1$ would mean that there is no systematic shift among two sets of data.

In this sense, our intensities agree on average with those of Toth [22] within 2–3% and with those of Mikhailenko et al. [19,60] within 3–4%. However, the intensities of Toth are systematically lower than ours, whereas those of Mikhailenko et al. [19,60], obtained from Giessen spectra are systematically higher. This important remark is to be correlated with the validation of the absolute intensities, particularly in the HITRAN database, confirmed through a comparison with the theoretical PS line lists based on variational calculations using pure *ab initio* dipole moment surfaces [46] and on the potential energy surface from [45] as cited before (see the next section for more details).

The last column in Table 10 shows the unweighted RMS deviation between the intensities of this work and those of the data sets available in the literature defined in a usual way

$$\mathrm{RMS} = \left\{ (N-1)^{-1} \sum_{i}^{N} (\Delta S_i / \bar{S}_i)^2 \right\}^{1/2}, \tag{6}$$

where $\Delta S_i = S_i^{\text{literature}} - S_i^{\text{our}}$ and $\bar{S}_i = (S_i^{\text{literature}} + S_i^{\text{our}})/2$, N is the number of lines in common. It is seen that the RMS vary from ~20% to 40% depending on the source of data. All the lines were included in the RMS calculations and the major contribution to these high values comes essentially (see Figs. 4–7) from weak lines or blended lines. For weaker lines, the scatter between our measured intensities and the literature data can reach a factor of 3 or even higher and there is still room for an improvement of databases and of theoretical models.

Note that our measurements cover the largest intensity range with respect to other available experimental data corresponding to Figs. 4(a)–(d): the weakest lines are missing in panels (a) and (b) [22,60]; strong lines are missing in panels (b) and (c) [21,60]; and panel (d) only contains strong lines [61]. The number of previously measured intensities in this wave number range compared to our data (in %) is given in the second column of Table 10.

For $H_2^{17}O$, the number of lines in common with literature data is relatively low and their intensities are lower than 10^{-23} cm/molecule. An excellent agreement is obtained (see Fig. 5) with the data of Mikhailenko et al.

Table 9
Number of assigned lines (N) and integrated intensities (ΣS_σ) at 296 K for the predominant bands of $H_2^{16}O$ and each isotopologue in the 4200–6600 cm^{-1} spectral range

	This work		Toth [22,32,33]		HITRAN [35][a]		Mikhailenko et al. [60][b,c]		PS [45,46][d]
	N	ΣS_σ (cm/molec)	N	$\Delta\Sigma S_\sigma$ (%)[e]	N	$\Delta\Sigma S_\sigma$ (%)[e]	N	$\Delta\Sigma S_\sigma$ (%)[e]	$\Delta\Sigma S_\sigma$ (%)[e]
$H_2^{16}O$									
0 1 1–0 0 0	1349	7.84×10^{-19}	1042	+5.1	1221	+6.0			+5.7
0 3 0–0 0 0	713	3.53×10^{-22}	475	+7.1	655	+9.6	510	−2.6	+26
1 1 0–0 0 0	1030	5.00×10^{-20}	750	+3.8	921	−24.7			−27.8
Total	5438	8.74×10^{-19}	3351	−1.5	4069	−0.5			+1.7
$H_2^{17}O$	576	2.97×10^{-22}	395	+1.3	763	+8.4	506	−6.8	+4.4
$H_2^{18}O$	1060	1.55×10^{-21}	532	+7.1	1269	+12.2	576	+16.1	+11.0
HDO	3087	1.96×10^{-22}			1815	−8.2	873	−19.4	−12.2
Unassigned	128	3.40×10^{-25}							
Total	10,161	8.76×10^{-19}			7916	−0.5			+1.7

[a]Mainly originates from Toth [22,32,33].
[b]All the lines whose intensities are $>8\times10^{-23}$ cm/molecule are not taken into account because they are saturated (see text).
[c]Unpublished intensity data from the measurements of Mikhailenko et al. [19] have been put at our disposal before publication [58].
[d]PS is referred to the calculation using the potential energy surface and the pure *ab initio* dipole moment surfaces of Schwenke and Partridge [45,46].
[e]$\Delta\Sigma_\sigma$ (%) is the percent difference compared to the present work.

[19,60] (panel b) obtained from Giessen spectra. This data set represents the most complete experimental set available for comparison (nearly 90% of measured lines are in common). The comparison with the data of Toth [22] (panel a) shows a two times larger RMS deviation while the values of Macko et al. [21] remains 11% lower than ours according to the R statistical criteria but the number of lines in common is small in the latter case. The comparison with the calculated data [46] shows that the present values are lower on average by 7%, with discrepancies increasing towards weaker lines.

Fig. 6 and Table 10 show that the values of $H_2^{18}O$ line intensities of the present work are generally lower than those of the literature except those of Macko et al. [21] for which the comparison, as above, might not be significant due to few common lines. The examination of the values of R and A leads to the conclusion that our values are slightly lower for the weak lines, when compared to the data of Chevillard et al. [25–27] obtained with enriched $H_2^{18}O$ samples. This result is also valid when the comparison with the calculated data [46] is considered.

Despite a poorer accuracy of our HDO line intensities, which is due to both the lower intensity range and the correction that was applied to take into account the residual deuterium concentration in the cell, a good agreement is obtained with the data of Toth [31,32] on the whole intensity range. The comparison with Mikhailenko et al. [60] shows more scattering while the values of Macko et al. [21] are, as for previously discussed isotopologues, lower than ours (Fig. 7 and Table 10).

4.2.2. Comparison with the theory

The only source available in the literature for all four isotopic species that provides a comparative sampling corresponds to global intensity predictions using variational methods. Comparisons with such calculations (available at http://spectra.iao.ru) generated with the dipole moment function of Schwenke and Partridge (SP) [45,46] are shown in the last panels of Figs. 4–7.

Based on the R and A statistical criteria, shown in Table 10, the agreement is very good, in particular for the principal isotopologue $H_2^{16}O$: only 1% deviation in the linear regression slope coefficient A for strong lines, and 2% deviation in the median line position R for the scatter of discrepancies (Fig. 4(e)). These criteria values

Table 10
Comparison of the line intensities with data of the literature

	N[a]	%[b]	Intensity range (cm/molecule)[a]	Spectral range (cm^{-1})[a]	R[c]	A[c]	RMS %[d]
$H_2{}^{16}O$							
Toth [22]	3343	64.4	8.6×10^{-28}–2.8×10^{-20}	4200–6600	0.98	1.03	23
Mikhailenko et al [60][e]	2937	56.6	2.1×10^{-27}–6.8×10^{-23}	4200–6600	1.03	0.96	30
Macko et al. [21]	858	16.5	1.2×10^{-29}–1.7×10^{-23}	6130–6600	1.25	0.88	31
Ptashnik et al. [61]	430	8.3	1.8×10^{-23}–2.8×10^{-20}	5037–5585	1.01	1.05	18
HITRAN 2004 [35]	3590	69.2	3.2×10^{-28}–2.8×10^{-20}	4200–6600	1.00	1.02	24
Schwenke and Partridge [46]	5100	#	1.2×10^{-29}–2.9×10^{-20}	4200–6600	1.02	0.99	30
$H_2{}^{17}O$							
Toth [22]	395	71.4	3.2×10^{-27}–1.1×10^{-23}	4200–5820	0.94	1.01	38
Mikhailenko et al [60][e]	501	90.6	3.2×10^{-28}–1.0×10^{-23}	4200–6600	0.99	1.01	16
Macko et al. [21]	19	3.4	1.2×10^{-29}–2.2×10^{-26}	6170–6600	1.11	0.96	40
HITRAN 2004 [35]	395	71.4	1.2×10^{-27}–1.1×10^{-23}	4200–5820	0.93	1.00	35
Schwenke and Partridge [46]	518	#	9.1×10^{-29}–1.1×10^{-23}	4200–6600	1.07	0.97	43
$H_2{}^{18}O$							
Toth [22]	531	51.5	4.1×10^{-27}–5.6×10^{-23}	4200–6600	0.90	0.94	27
Mikhailenko et al [60][e]	576	55.9	1.2×10^{-27}–6.1×10^{-23}	4200–6600	0.87	0.87	32
Macko et al. [21]	64	6.2	1.2×10^{-29}–4.3×10^{-26}	6130–6600	1.27	0.96	36
Chevillard et al. [25–27]	859	83.3	3.8×10^{-27}–5.6×10^{-23}	4430–6090	0.93	0.94	34
HITRAN 2004 [35]	754	73.1	3.8×10^{-27}–5.6×10^{-23}	4200–6600	0.93	0.97	32
Schwenke and Partridge [46]	986	#	3.7×10^{-29}–5.7×10^{-23}	4200–6600	0.95	0.92	36
HDO							
Toth [32,33]	1801	63.6	1.5×10^{-28}–1.6×10^{-24}	4720–6600	1.01	1.11	24
Mikhailenko et al [60][e]	852	30.1	2.0×10^{-27}–2.1×10^{-24}	4200–6540	1.33	0.84	45
Macko et al. [21]	982	34.7	2.4×10^{-30}–3.1×10^{-25}	6130–6600	1.35	0.83	49
HITRAN 2004 [35]	1352	47.7	8.6×10^{-28}–1.5×10^{-24}	4200–6600	1.08	0.85	24
Schwenke and Partridge [46]	2718	#	1.8×10^{-29}–2.1×10^{-24}	4200–6600	1.11	1.01	37

The global calculations are, by definition, complete with few missing comparisons (see text). They contain all allowed transitions up to 10^{-30} cm/molecule. However, about 3% of the total number of lines has been excluded from the intensity comparison when the lines were overlapped in the observed spectra by other molecules or isotopologues.

[a] N is the number of lines in common with this work and the literature. The intensity and the spectral ranges are again those in common with this work.

[b] % is the N(literature) / N(this work) percent ratio in the full spectral range of this work.

[c] R is the mean value of the ratios S_σ (this work)/S_σ (literature) and A is the regression coefficient of the plots S_σ (this work) = $A\times S_\sigma$ (literature) where S_σ is the line intensity.

[d] RMS is the unweighted root-mean square deviation between intensities in this work and literature data.

[e] Same remarks as in Table 9.

slightly degrade for the other isotopologues: up to 9% for the A-value of $H_2^{18}O$ and up to 11% of the R-value of HDO. The unweighted RMS deviation is 30% for $H_2^{16}O$ increasing for other isotopologues up to 43% for $H_2^{17}O$, which should be considered as a generally good agreement taking into account the fact that SP calculations were carried out from pure *ab initio* dipole moment surfaces and that the comparison covers an extremely large intensity interval from 1.2×10^{-29} to 2.9×10^{-20} cm/molecule.

Also, the uncertainty of the experimental intensity determination increases for weak, blended and overlapping lines and can hardly be evaluated due to the well-known difficulty of measurements in such cases.

However, a closer examination into a given vibrational band shows some significant intensity outliers for weak lines forming in some cases systematic series. An example for $K''=0$ (a) and $K''=1$ (b) series of the $3\nu_2$ band of $H_2^{16}O$ is given in Fig. 8. A systematic deviation with the change of sign for outliers occurs in this case between 4600 and 5000 cm^{-1} (open squares in (a) and (b) panels). Similar deviations are observed for some other series. During the course of this work, we were aware of a new variational calculation of Tashkun et al. [62] (hereafter referred to as TST calculations). These calculations have been performed with extended cut-off for the number of basis wave functions and extended matrix dimensions for Hamiltonian symmetry blocks

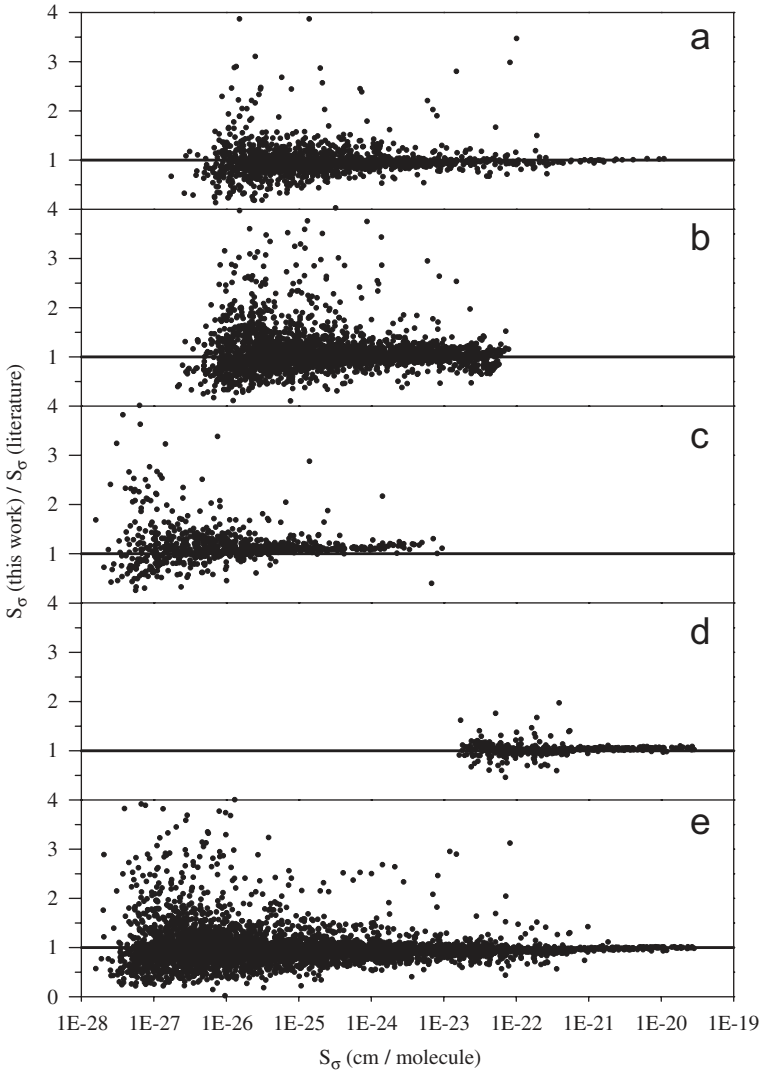

Fig. 4. Line by line comparison of the $H_2^{16}O$ intensities with the experimental (a–d) and calculated values found in the literature: (a) Toth [22], (b) Mikhailenko et al. [19,60], (c) Macko et al. [21], (d) Ptashnik et al. [61], (e) Schwenke and Partridge [46]. The horizontal line is shown as a landmark.

and using new dipole moment surfaces simultaneously optimized with respect to *ab initio* calculations and empirical intensity (which has not yet been included in our data). Fig. 8 (full triangles) shows a better agreement of these new predictions with the measurements of the present study.

4.3. Self-broadening parameters

In the line list, 7832 self-broadening coefficients for the four isotopologues have been determined for a total of 10394 lines. As stated before, γ_{self} values are given when the Lorentzian contribution is well defined (value $>3\sigma$ uncertainty). So, γ_{self} values vary from 0.0415 to 0.847 cm^{-1}/atm. Among these coefficients, 4466 belong to $H_2^{16}O$ and can be compared to the 3351 smoothed values of Toth [34 and references therein] obtained using semi-empirical functions for the fits of the widths in terms of "families" of rotational transitions in the region between 2800 and 8000 cm^{-1}. The comparison between the two data sets (3221 values in common) reveals that Toth's values are in the range 0.100–0.513 cm^{-1}/atm while some of ours are outside this interval, likely caused

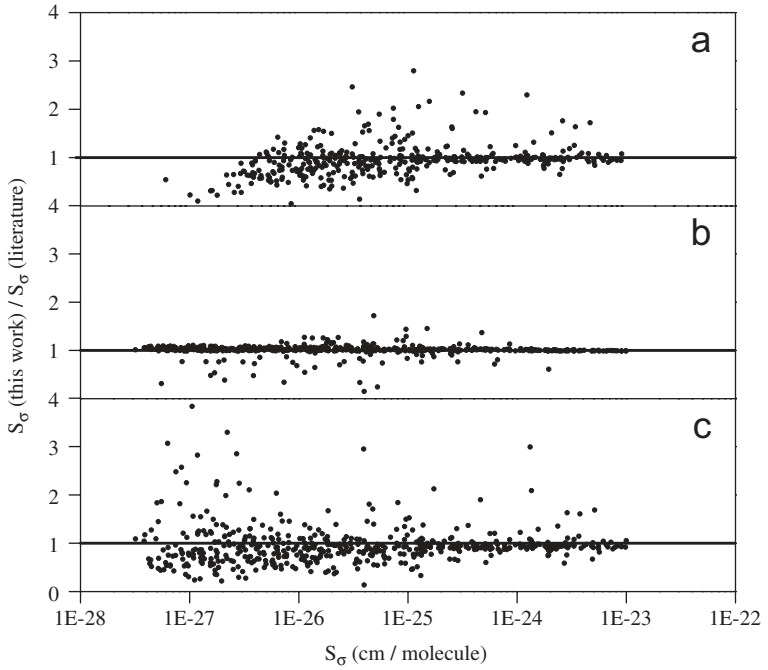

Fig. 5. Line by line comparison of the $H_2^{17}O$ intensities with the (a and b) experimental and (c) calculated literature data: (a) Toth [22], (b) Mikhailenko et al. [19,60] and (c) Schwenke and Partridge [46]. The horizontal line is shown as a landmark.

by the measurement of blended features. The mean values are very close to each other (0.341 and 0.342 cm^{-1}/atm for this work and Toth, respectively). The mean ratio γ_{self} (this work)/γ_{self} (Toth) = 0.99 also reflects the good agreement between the two data sets and consequently between our values and the HITRAN database constituted by the experimental parameters of Ref. [63] and the smoothed data of Toth [34]. Fig. 9 illustrates this comparison for the common lines in the 011–00, 030–000 and 110–000 bands with $\Delta K_a = 0, \pm 1$ drawn vs. K_m and J_m as in [64]. Another set of values focusing on stronger lines in the restricted region 5000–5600 cm^{-1} [61] is also compared in the same figure. Their values are on average slightly lower than ours (mean ratio = 1.04).

For the other isotopologues, the γ_{self} values are much more difficult to obtain due to the weakness of the lines (see Table 10) because of the low partial pressures in the natural water vapor. The comparison with the HITRAN compilation is, therefore, less efficient. Nevertheless, 382 values for $H_2^{17}O$, 797 for $H_2^{18}O$ and 2291 for HDO have been determined and mean ratios γ_{self} (This work)/γ_{self} (Toth) very close to unity were obtained (0.97, 1.02 and 1.02 for $H_2^{17}O$, $H_2^{18}O$ and HDO, respectively). No significant differences between the isotopologues were observed, which tends to confirm the lack of isotopic dependence as suggested by the theoretical work of Gamache and Fischer [65].

4.4. Air-broadening and air-induced shift parameters

Out of the 4915 values of γ_{air} determined for the four isotopologues, 2950 belong to the main isotopologue $H_2^{16}O$. The number of values is slightly lower than for the self-broadening parameters due to the tendency of the weak lines to disappear at high total pressures. They cover a large range from 0.003 to 0.198 cm^{-1}/atm and give a mean value of 0.066 cm^{-1}/atm, which is in very good agreement with the mean value of 0.065 cm^{-1}/atm reported by Toth [34]. The comparison of the 2623 values in common with the same author leads to a mean ratio [γ_{air} (this work)/γ_{air} (Toth)] equal to 0.99. The comparison of our values with the corresponding HITRAN values is illustrated in Fig. 10.

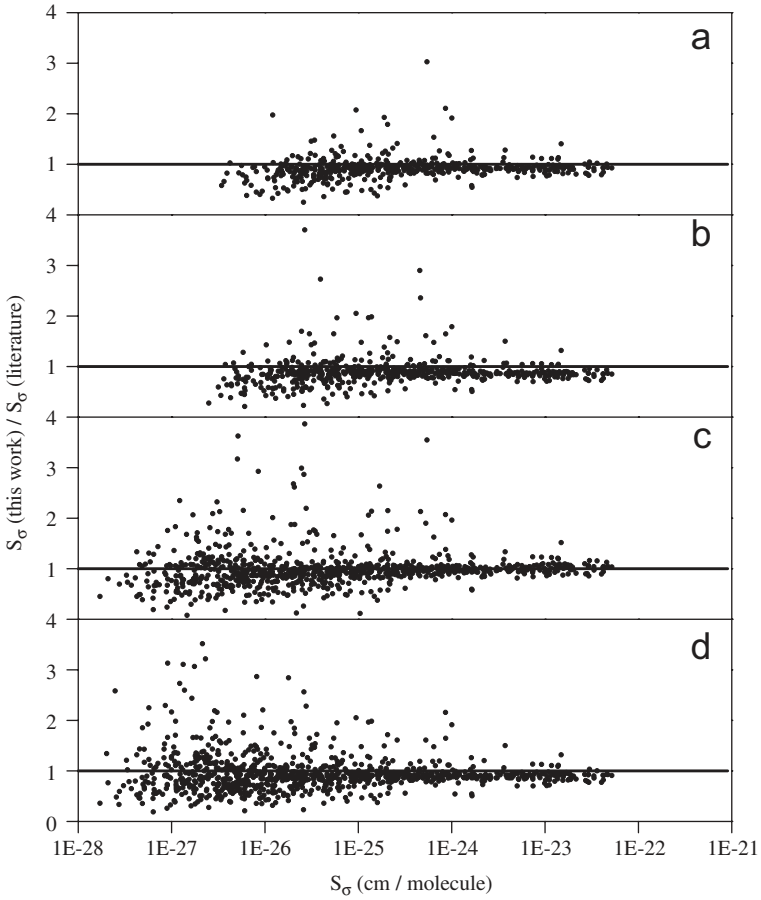

Fig. 6. Line-by-line comparison of the $H_2^{18}O$ intensities with the (a–c) experimental and (d) calculated values found in the literature: (a) Toth [22]; (b) Mikhailenko et al. [19,60]; (c) Chevillard et al. [25–27] (d) Schwenke and Partridge [46]. The horizontal line is shown as a landmark.

The latter corresponds to semi-empirical values recently obtained by Jacquemart et al. [66]. This calculation, describing the vibrational dependence of the air-broadened half-widths and air-induced pressure shifts, is based on fits of theoretical data from the expansion of the complex Robert–Bonamy (CRB) equations and selected experimental data from the microwave region to the visible (see references in [66]). In particular, the data reported by Toth [34] after his smoothing procedure are implicitly included in the HITRAN database. The slope of the plot A and the mean ratio R are very close or equal to unity ($A = 1.02$ and $R = 1.00$), demonstrating a very good agreement between both data sets. Moreover, the comparisons with the data of Toth [34] and with the data of HITRAN [35] give quite the same conclusions. We can, therefore, stay confident with the proposed values, which can be described, as noted in Ref. [66], by semi-empirical functions dependent on vibrational quantum numbers [66] as well as rotational quantum numbers [34].

The air-broadening parameters γ_{air} have also been determined for the $H_2^{17}O$, $H_2^{18}O$ and HDO isotopologues. As noted before, the number of values is much less than in the case of $H_2^{16}O$: 155, 392 and 1476 values, respectively. These values have been compared to their corresponding HITRAN values where the data of Ref. [66] are considered for $H_2^{17}O$ and $H_2^{18}O$ and those of Ref. [34] for HDO. A good agreement was obtained in spite of the small number of values, the mean ratios being 0.96, 0.98 and 1.03, respectively.

The air-induced shift parameters δ_{air} of the water vapor spectral lines are quantities as essential as the air-broadening parameters in databases for atmospheric remote-sensing experiments. It is now recognized that they are much more difficult to obtain and values reported by different laboratories significantly disagree.

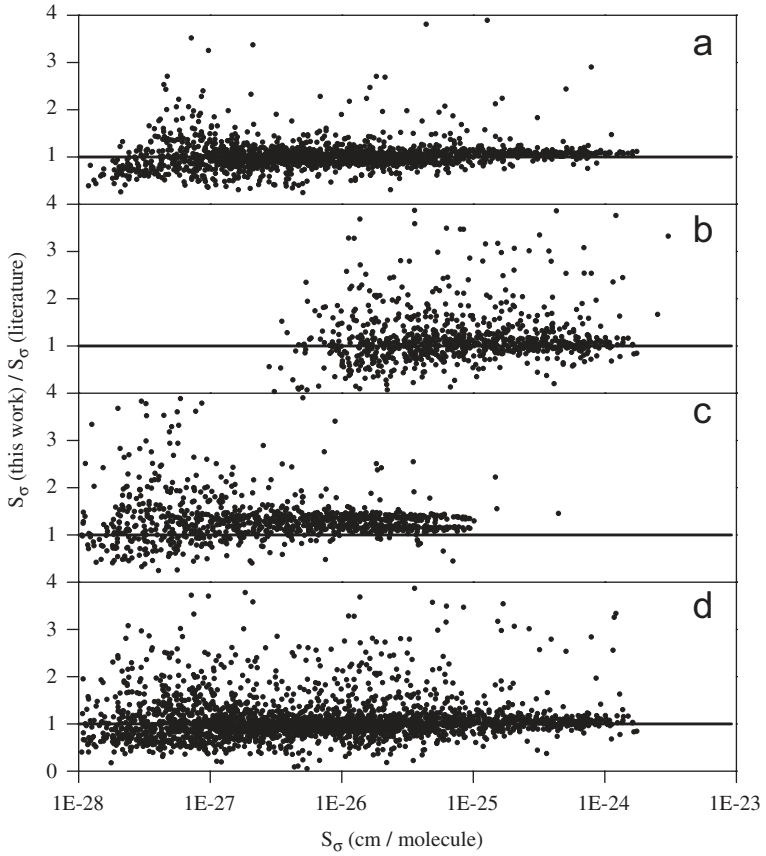

Fig. 7. Line by line comparison of the HDO intensities with the (a, b, c) experimental and (d) calculated values found in the literature: (a) Toth [31,32]; (b) Mikhailenko et al. [19,60]; (c) Macko et al. [21]; and (d) Schwenke and Partridge [46]. The horizontal line is shown as a landmark.

Comparisons with the HITRAN database would be of prime interest. In the present work, 4913 δ_{air} values are reported and among them, 2778 values belong to $H_2^{16}O$. They are compared to the HITRAN values in Fig. 11(a) (all common lines) and Fig. 11(b) (common lines of the 011, 030 and 110 bands with $\Delta K_a = 0, \pm 1$). Most of the lines are shifted towards smaller wave numbers and the shifts become larger with increasing JK_m values. It must be noted that the HITRAN data set is that of the semi empirical approach of Ref. [66] implicitly including the line shifts reported by Toth [34] after his smoothing procedure as for γ_{air} parameters. If small differences between the HITRAN data set [35] and the Toth's subset [34] remain as shown in Fig. 11(b), the agreement between both data sets is fairly good in view of the difficulty to obtain the parameters. Similar agreements are observed for $H_2^{17}O$ and $H_2^{18}O$ isotopologues whereas no comparison can be made with HITRAN for HDO because of the lack of values.

The above comparisons show that discrepancies remain between different experimental measurements of the broadening and shift parameters and further work is in progress to properly analyze them in detail for the different isotopologues.

4.5. Water vapor data base

The present measurements of line parameters extend the Brussels-Reims (BR) water vapor database, which previously covered the spectral region 26000–9250 cm^{-1} with a large dynamic range of line intensities. This study was performed with natural water vapor, i.e. with all the isotopologues present in natural abundances.

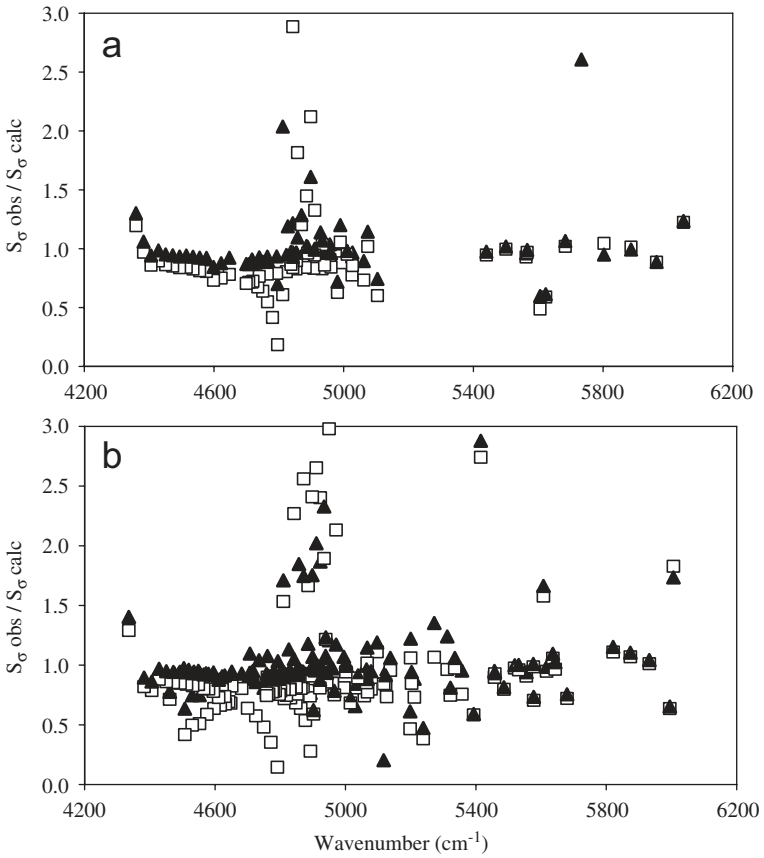

Fig. 8. Comparison of the $H_2^{16}O$ line intensities measured in this work and variational calculations from dipole moment surfaces in the (0 3 0)–(0 0 0) band for the series (a) $K'' = 0$ and (b) $K'' = 1$. Open squares correspond to discrepancies with SP calculations [46] and open triangles correspond to discrepancies with TST calculations [62].

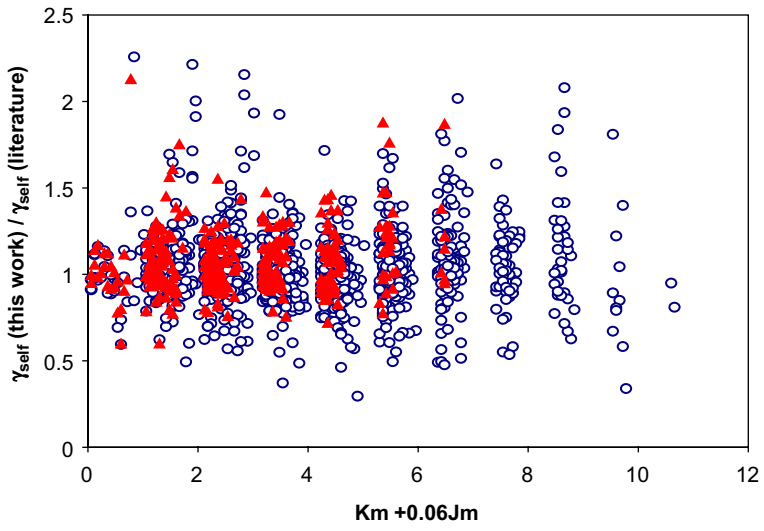

Fig. 9. Comparison of the self-broadening coefficients of $H_2^{16}O$ in the (0 1 1)–(0 0 0), (0 3 0–0 0 0) and (1 1 0–0 0 0) bands with $\Delta K_a = 0, \pm 1$ obtained in this work with the data of Toth [34] (open circles) and Ptashnik et al. [61] (full triangles).

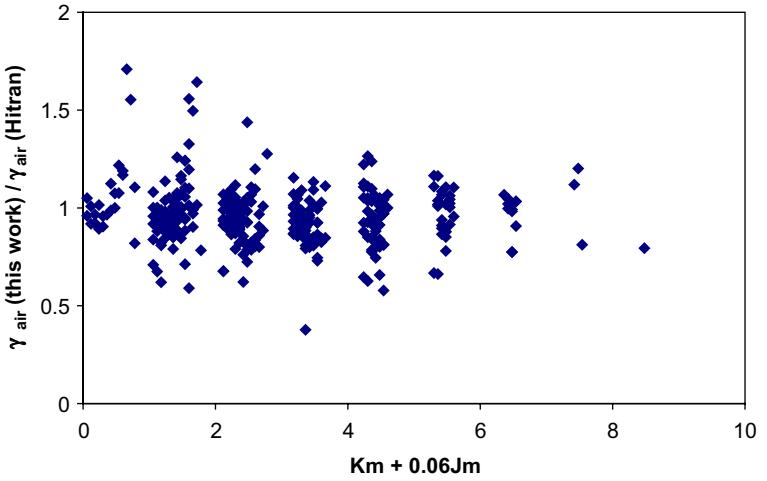

Fig. 10. Comparison of the air-broadening coefficients of $H_2^{16}O$ in the (0 1 1)–(0 0 0), (0 3 0)–(0 0 0) and (1 1 0)–(0 0 0) bands with $\Delta K_a = 0, \pm 1$ obtained in this work with the data of HITRAN [35].

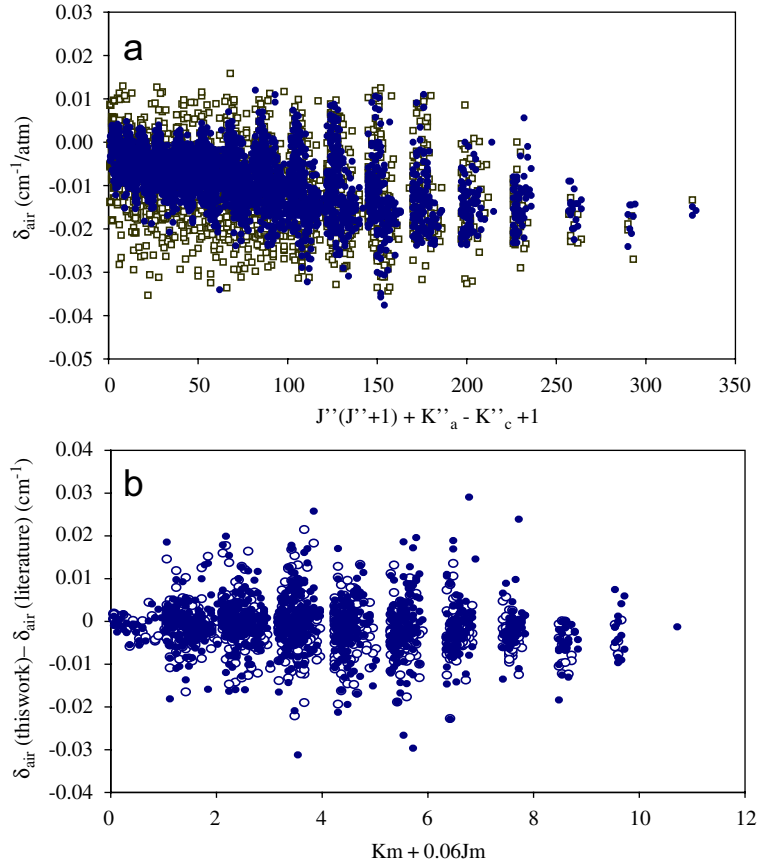

Fig. 11. Comparison of the pressure-induced shifts δ_{air} of the $H_2^{16}O$ lines with literature data: (a) Data are plotted against an energy-ordered index $J''(J''+1)+K_a''-K_c''+1$: this work (open squares), HITRAN (full circles), (b) Observed differences with the literature data: Toth [34] (open circles), HITRAN (full circles) in the (0 1 1–0 0 0), (0 3 0–0 0 0) and (1 1 0–0 0 0) bands with $\Delta K_a = 0, \pm 1$.

Even if some studies have been made with isotopically enriched water, the number of lines included in the HITRAN database is not more extensive than in the BR database. As a result of the present contribution, 3280 lines of the four $H_2^{16}O$, $H_2^{17}O$, $H_2^{18}O$ and HDO isotopologues with low intensity are observed for the first time (see Fig. 12). The insertion of such lines in HITRAN would be useful for atmospheric and astrophysical applications. It is especially required in the "atmospheric windows" in the spectral regions 4200–5000 and 5800–6600 cm^{-1} where the water lines can interfere with weak features of trace gases to be detected. Although the respective contributions of these new lines is less than 0.3% and 1.5% of the total intensity in these two spectral regions, they contribute significantly to the atmospheric attenuation in some specific regions (9.2% of the total intensity in the 6120–6260 cm^{-1} spectral range as shown in Fig. 12 as already stated by Macko et al. [21]). Conversely, 874 lines (269 for $H_2^{16}O$, 199 for $H_2^{17}O$, 267 for $H_2^{18}O$, 139 for HDO) listed in the HITRAN database with intensities lower than 10^{-25} cm/molecule do not appear in our pure water absorption spectra. They probably result from calculations and differ noticeably in position and/or in intensity from the observed ones. Further improvements should be gained to assert their validity.

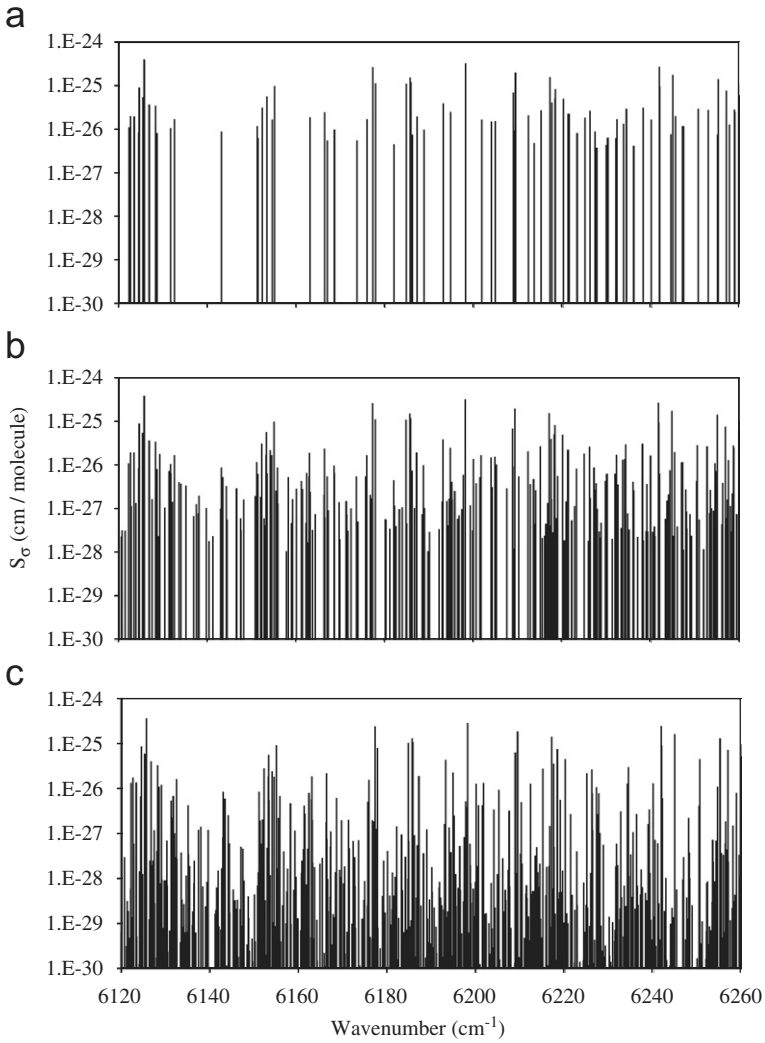

Fig. 12. Stick spectrum of the H_2O vapor lines in the 6120–6260 cm^{-1} spectral region of the atmospheric window drawn with the data of (a) HITRAN [35], (b) this work and (c) theoretical calculation [62].

5. Conclusion

In the 4200–6600 cm^{-1} spectral region, a new set of water vapor line parameters has been reported, extending our previous studies on the absorption spectrum in the near infrared and visible regions. Accurate measurements were performed on a wide range of line intensities (10^{-29}–10^{-19} cm/molecule) by means of high-resolution Fourier transform spectrometers coupled to three different cells allowing absorption paths from 0.3 to 1800 m. Special attention was put on the detection of very weak lines with the longest absorption paths. Spectra under various conditions of path-length, pressure and in presence of air have been recorded to determine the positions, the intensities, the self- and air-broadening coefficients and the pressure-induced shifts of about 10,400 lines belonging to the four isotopologues $H_2^{16}O$, $H_2^{17}O$, $H_2^{18}O$ and HDO. The comparison with HITRAN has shown that about 3280 weak lines are not reported in the latest version of the HITRAN-2004 database [35]. These lines give rise to the assignments of 53 new energy levels of the (0 0 1), (0 3 0) and (1 1 0) states for $H_2^{17}O$, 9 new energy levels of the (0 0 1) and (1 0 0) states for $H_2^{18}O$ and 74 new energy levels of the (0 1 1), (0 4 0), (1 1 0), (1 2 0) and (2 0 0) states for HDO.

Intensities have been measured for all observed lines, more than 30% of them being determined experimentally for the first time. For common sets of measurements, our intensity data agrees well on average with previous experimental works [21,22,25–27,60,61] particularly for strong and medium lines. A detailed comparison with literature results has been done including the examination of the averaged A and R statistical criteria: the linear regression coefficient (A) and the median of intensity ratios distribution (R) that provide information on absolute intensity calibrations among various data sources. According to these criteria our intensities lie on average between Toth values [22] (+2% to +3%) and those of Mikhailenko et al. [60] (−3 to −4%), which were previously the most extended experimental investigations in this range. An excellent agreement has been observed with *ab initio* intensity predictions of SP [46] (+1 to +2%) again according to R and A criteria.

However, for weaker lines the scatter of discrepancies between our measured intensities and the previously available data (both experimental and theoretical) generally increases, resulting in overall standard deviations of ~20–40% depending on the isotopologue. There is still place for an improvement of databases and of theoretical models. Some progress in this direction has been recently achieved via an optimization of dipole moment function [62] using simultaneously *ab initio* and experimental data.

The self- and air-broadening coefficients, as well as the air-induced shifts, obtained for a large number of lines, were shown to be in good agreement with semi-empirical values listed in the HITRAN database. This confirms, in this wavenumber range, an absolute calibration for these line parameters present in HITRAN and GEISA/IASI databases that have been compiled by merging independent measurements and calculated values. But they could be completed with new data obtained in this work. Also our experimental spectra do not confirm some water lines included in the existing databases.

The present work should improve atmospheric studies investigating this important spectral region, as the newly observed weak lines could be of the utmost importance for remote sensing measurements.

Acknowledgments

We are grateful for the support provided by the Centre National de Recherche Scientifique (CNRS, France), the Institut National des Sciences de l'Univers (INSU, France) through the Programme National de Chimie Atmosphérique (PNCA).

This research program was also supported by the Belgian Federal Science Policy Office (contract EV/11/03C), the Fonds National de la Recherche Scientifique (FNRS, Belgium) and the European Space Agency (ESA-Prodex program).

SM thanks the financial support from the Centre National de Recherche Scientifique (France) and the Russian Foundation of Basic Researches (Russia) in the frame of grant PICS no. 05-05-22001. This position was also partly supported by the scientific school of Prof. S.D. Tvorogov "Optical Spectroscopy of Molecules and Radiative Processes in the Atmosphere" (the National Program РИ-112/001/020). V.T. thanks D. Schwenke and S.Tashkun for collaborations in global calculations and acknowledges support from the IDRIS computer center of CNRS.

This research forms part of an effort by a task group of the IUPAC (Project no. 2004-035-1-100) to compile, determine and validate, both experimentally and theoretically, accurate frequencies, energy levels, line intensities, line widths and pressure effect spectral parameters of all major isotopologues of water.

Appendix A

For the observed ground state energy levels from [45] used to calculate the new upper state levels, see Table A.1.

Table A.1
Ground state experimental energy levels of the HDO, $H_2^{18}O$ and $H_2^{17}O$ molecules (in cm^{-1})

J	K_a	K_c	HDO	dE	$H_2^{18}O$	dE	$H_2^{17}O$	dE
1	0	1	15.5083	1	23.7549	2	23.7735	1
1	1	1	29.8084	1	36.7486	2	36.9311	1
1	1	0	32.4963	1	42.0233	2	42.1869	1
2	0	2	46.1731	1	69.9275	1	70.0047	1
2	1	2	58.1268	1	78.9885	1	79.2274	1
2	1	1	66.1843	1	94.7885	1	94.9706	1
2	2	1	108.9261	1	133.4756	1	134.1452	1
2	2	0	109.2691	1	134.7830	1	135.4312	1
3	0	3	91.3301	1	136.3365	1	136.5377	1
3	1	3	100.3908	1	141.5680	1	141.9024	1
3	1	2	116.4613	1	172.8827	1	173.1101	1
3	2	2	155.3889	1	204.7559	1	205.4818	1
3	2	1	157.0646	1	210.7990	1	211.4358	1
3	3	1	233.0237	1	282.0945	1	283.5616	1
3	3	0	233.0511	1	282.3070	1	283.7677	1
4	0	4	150.1563	1	221.2339	1	221.6209	1
4	1	4	156.3821	1	223.8283	1	224.3043	1
4	1	3	182.9834	1	274.8031	1	275.1306	1
4	2	3	217.0419	1	298.6199	1	299.4389	1
4	2	2	221.8360	1	314.4593	1	315.0786	1
4	3	2	295.4873	1	379.2914	1	380.8058	1
4	3	1	295.6774	1	380.7024	1	382.1760	1
4	4	1	402.3293	1	482.6435	1	485.2090	1
4	4	0	402.3309	1	482.6725	1	485.2369	1
5	0	5	221.9461	1	324.0465	1	324.6610	1
5	1	5	225.8648	1	325.2157	1	325.8802	1
5	1	4	265.2362	1	398.3603	1	398.8793	1
5	2	4	293.6365	1	414.1681	1	415.1280	1
5	2	3	303.9948	1	445.1583	1	445.7934	1
5	3	3	373.6659	1	500.5961	1	502.1797	1
5	3	2	374.4099	1	505.7286	1	507.1743	1
5	4	2	480.2426	1	604.5442	1	607.1592	1
5	4	1	480.2588	1	604.7927	1	607.3974	1
5	5	1	615.9686	1	733.6794	1	737.6204	1
5	5	0	615.9688	1	733.6827	1	737.6238	1
6	0	6	306.3147	1	444.8461	1	445.7191	1
6	1	6	308.6156	1	445.3460	1	446.2450	1
6	1	5	362.5071	1	541.1800	1	541.9968	1
6	2	5	384.8754	1	550.4507	1	551.6093	1
6	2	4	403.5489	1	601.2377	1	601.9608	1
6	3	4	467.5144	1	645.3824	1	647.0721	1
6	3	3	469.6635	1	658.6099	1	659.9867	1
6	4	3	573.8906	1	751.0328	1	753.7050	1
6	4	2	573.9706	1	752.1874	1	754.8117	1
6	5	2	709.1666	1	880.0762	1	884.0775	1

Table A.1 (*continued*)

J	K_a	K_c	HDO	dE	$H_2^{18}O$	dE	$H_2^{17}O$	dE
6	5	1	709.1674	1	880.1144	1	884.1137	1
6	6	1	872.7905	1	1033.1939	1	1038.7649	1
6	6	0	872.7905	1	1033.1946	1	1038.7652	1
7	0	7	403.1614	1	583.7777	1	584.9408	1
7	1	7	404.4455	1	583.9862	1	585.1619	1
7	1	6	473.9176	1	701.6942	1	702.8858	1
7	2	6	490.4273	1	706.5975	1	708.0163	1
7	2	5	520.1234	1	780.4526	1	781.3773	1
7	3	5	576.9046	1	812.7617	1	814.6106	1
7	3	4	581.9619	1	839.5495	1	840.8648	1
7	4	4	683.3239	1	921.8957	1	924.6414	1
7	4	3	683.6100	1	925.6997	1	928.2958	1
7	5	3	818.0066	1	1050.9901	1	1055.0539	1
7	5	2	818.0135	1	1051.2030	1	1055.2550	1
7	6	2	981.1279	1	1204.1693	1	1209.8132	1
7	6	1	981.1279	1	1204.1745	1	1209.8182	1
7	7	1	1171.5313	1	1378.9866	1	1386.4185	2
7	7	0	1171.5314	1	1378.9865	1	1386.4187	1
8	0	8	512.5157	1	740.9122	1	742.3985	1
8	1	8	513.2071	1	740.9986	1	742.4908	1
8	1	7	598.5630	1	879.4945	1	881.0989	1
8	2	7	609.9464	1	881.9140	1	883.6519	1
8	2	6	653.0886	1	980.2221	1	981.4958	1
8	3	6	701.6202	1	1001.7056	1	1003.7811	1
8	3	5	711.7953	1	1047.3285	1	1048.6569	1
8	4	5	808.5630	1	1116.6361	1	1119.4879	1
8	4	4	809.3931	1	1126.4390	1	1128.9380	1
8	5	4	942.5323	1	1246.3685	1	1250.4985	1
8	5	3	942.5619	1	1247.2058	1	1251.2909	1
8	6	3	1105.0035	1	1399.4279	1	1405.1478	1
8	6	2	1105.0038	1	1399.4632	1	1405.1808	1
8	7	2	1294.8364	1	1574.6777	1	1582.1963	1
8	7	1	1294.8364	1	1574.6780	2	1582.1968	2
8	8	1	1510.8785	2	1768.8019	2	1778.3071	2
8	8	0	1510.8786	2	1768.8016	2	1778.3078	2
9	0	9	634.4279	1	916.2578	1	918.1019	1
9	1	9	634.7908	1	916.2931	1	918.1404	1
9	1	8	735.7350	1	1074.7629	1	1076.8008	1
9	2	8	743.0972	1	1075.9091	1	1078.0202	1
9	2	7	801.6438	1	1198.1995	1	1199.9630	1
9	3	7	841.3675	1	1211.1855	1	1213.5623	1
9	3	6	859.3924	1	1279.7975	1	1281.2684	1
9	4	6	949.5773	1	1334.4789	1	1337.4893	1
9	4	5	951.6355	1	1355.1992	1	1357.5555	1
9	5	5	1082.7849	1	1466.0182	1	1470.2254	1
9	5	4	1082.8863	1	1468.6122	1	1472.6846	1
9	6	4	1244.4373	1	1618.8962	1	1624.6935	1
9	6	3	1244.4394	1	1619.0558	1	1624.8419	1
9	7	3	1433.5719	1	1794.3749	2	1801.9849	2
9	7	2	1433.5716	1	1794.3802	1	1801.9899	1
9	8	2	1648.9470	2	1989.3521	3	1998.9560	2
9	8	1	1648.9470	2	1989.3524	2	1998.9562	2
9	9	1	1889.5071	2	2200.4070	5		
9	9	0	1889.5071	2	2200.4070	3		
10	0	10	768.9299	1	1109.7869	2	1112.0247	2
10	1	10	769.1166	1	1109.8020	1	1112.0408	1
10	1	9	885.0643	1	1287.7346	1	1290.2281	1
10	2	9	889.5755	1	1288.2672	1	1290.7985	1

Table A.1 (*continued*)

J	K_a	K_c	HDO	dE	$H_2^{18}O$	dE	$H_2^{17}O$	dE
10	2	8	964.8503	1	1433.0286	1	1435.3671	1
10	3	8	995.7932	1	1440.2880	1	1443.0408	1
10	3	7	1024.5683	1	1534.3680	1	1536.1566	2
10	4	7	1106.2641	1	1574.4495	1	1577.6882	1
10	4	6	1110.7596	1	1611.6533	1	1613.9009	1
10	5	6	1238.7943	1	1709.5401	1	1713.8494	1
10	5	5	1239.0891	1	1716.1998	1	1720.1840	2
10	6	5	1399.4501	1	1862.4549	1	1868.3303	1
10	6	4	1399.4606	1	1863.0200	1	1868.8588	2
10	7	4	1587.7400	1	2037.9337	1	2045.6386	2
10	7	3	1587.7401	1	2037.9617	2	2045.6643	2
10	8	3	1802.3355	2	2233.6028	1		
10	8	2	1802.3362	2	2233.6029	2		
10	9	2	2042.1051	4				
10	9	1	2042.1051	2				
11	0	11	916.0287	1	1321.4543	2	1324.1217	2
11	1	11	916.1237	1	1321.4601	2	1324.1281	2
11	1	10	1046.4739	1	1518.5426	1	1521.5173	2
11	2	10	1049.1241	1	1518.7876	2	1521.7822	2
11	2	9	1141.6913	1	1684.4394	1	1687.3829	1
11	3	9	1164.5095	1	1688.2861	2	1691.4851	2
11	3	8	1206.7543	1	1808.3623	1	1810.6670	1
11	4	8	1278.4380	1	1835.4865	2	1839.0374	2
11	4	7	1287.2386	1	1894.1957	1	1896.4551	2
11	5	7	1410.5665	1	1976.2972	2	1980.7538	2
11	5	6	1411.3198	1	1990.8570	2	1994.6640	2
11	6	6	1570.0615	1	2129.8979	2	2135.8588	2
11	6	5	1570.0961	1	2131.5661	1	2137.4193	2
11	7	5	1757.3412	1	2305.1955	2		
11	7	4	1757.3417	1	2305.3064	2		
11	8	4	1971.0301	2				
11	8	3	1971.0302	2				
11	9	3	2209.9057	2				
11	9	2	2209.9055	2				
12	0	12	1075.7144	1	1551.2017	2	1554.3345	2
12	1	12	1075.7621	1	1551.2049	2	1554.3375	2
12	1	11	1220.0285	1	1767.2251	2	1770.7120	2
12	2	11	1221.5369	1	1767.3388	2	1770.8350	2
12	2	10	1331.2167	1	1952.6779	2	1956.2350	2
12	3	10	1347.1198	1	1954.6538	2	1958.3582	2
12	3	9	1405.1253	1	2099.5621	2	2102.5540	2
12	4	9	1465.8293	1	2116.5648	2	2120.5158	2
12	4	8	1481.4434	1	2200.4382	2	2202.8974	2
12	5	8	1598.0681	1	2265.4388	2		
12	5	7	1599.7997	1	2293.0093	2		
12	6	7	1756.2854	1	2420.8853	2		
12	6	6	1756.3845	1	2425.1239	2		
12	7	6	1942.3724	2	2595.9751	2		
12	7	5	1942.3757	2	2596.3380	4		
13	0	13	1247.9639	1	1798.9656	3	1802.5988	2
13	1	13	1247.9879	1	1798.9658	3	1802.5999	4
13	1	12	1405.8180	1	2033.7656	2	2037.7962	2
13	2	12	1406.6564	1	2033.8172	2	2037.8536	3
13	2	11	1532.7318	1	2238.0323	2	2242.2119	2
13	3	11	1543.2436	1	2239.0299	3	2243.2933	3
13	3	10	1618.7002	1	2406.7701	2	2410.5410	2
13	4	10	1668.0958	1	2416.7839	4		
13	4	9	1693.4438	2	2527.6889	2		

Table A.1 (*continued*)

J	K_a	K_c	HDO	dE	$H_2^{18}O$	dE	$H_2^{17}O$	dE
13	5	9	1801.2072	1	2575.9715	2		
13	5	8	1804.8397	1	2622.0101	3		
13	6	8	1958.1246	1	2734.8964	4		
13	6	7	1958.3830	1	2744.3453	2		
13	7	7	2142.8290	2				
13	7	6	2142.8401	2				
14	0	14	1432.7458	2	2064.6724	4	2068.8429	5
14	1	14	1432.7581	2	2064.6731	3	2068.8435	4
14	1	13	1603.9051	1	2318.1137	3	2322.7158	7
14	2	13	1604.3634	1	2318.1383	3	2322.7487	3
14	2	12	1745.8964	2	2540.6704	4	2545.4907	4
14	3	12	1752.5374	1	2541.1730	3		
14	3	11	1846.4020	1	2729.7670	5		
14	4	11	1884.8420	1				
14	4	10	1922.8878	2				
14	5	10	2019.8219	2				
14	5	9	2026.8313	2				
15	0	15	1630.0239	2	2348.2463	4		
15	1	15	1630.0297	2	2348.2457	5		
15	1	14	1814.3187	2	2620.2027	6		
15	2	14	1814.5654	2	2620.2142	9		
15	2	13	1970.6607	2				
15	3	13	1974.7076	2				
15	3	12	2087.1385	2				
15	4	12	2115.6439	2				
15	4	11	2169.0589	2				
16	0	16	1839.7564	3				
16	1	16	1839.7581	3				
16	1	15	2037.0580	2				
16	2	15	2037.1895	2				
16	2	14	2207.1156	2				
16	3	14	2209.5153	2				
16	3	13	2339.9443	2				
17	0	17	2061.8960	3				
17	1	17	2061.8988	3				
17	1	16	2272.1018	3				
17	2	16	2272.1717	3				
17	2	15	2455.3780	3				
18	0	18	2296.3984	4				
18	1	18	2296.3985	4				
18	1	17	2519.4154	4				
18	2	17	2519.4545	4				

Uncertainties on the energy levels (dE) are given in $10^{-4}\,cm^{-1}$ units

References

[1] Bernath PF. The spectroscopy of water vapour: experiment, theory and applications. Phys Chem Chem Phys 2002;4:1501–9.

[2] Coheur PF, Fally S, Carleer M, Clerbaux C, Colin R, Jenouvrier A, et al. New water vapor line parameters in the 26000–13000 cm^{-1} region. JQSRT 2002;74:493–510.

[3] Fally S, Coheur PF, Carleer M, Clerbaux C, Colin R, Jenouvrier A, et al. Water vapor line broadening and shifting by air in the 26000–13000 cm^{-1} region. JQSRT 2003;82:119–31.

[4] Mérienne MF, Jenouvrier A, Hermans C, Vandaele AC, Carleer M, Clerbaux C, et al. Water vapor line parameters in the 13000–9250 cm^{-1} region. JQSRT 2003;82:99–117.

[5] Tolchenov RN, Naumenko O, Zobov NF, Shirin SV, Polyansky OL, Tennyson J, et al. Water vapour line assignments in the 9250–26000 cm^{-1} frequency range. J Mol Spectrosc 2005;233:68–76.

[6] Pugh LA, Narahari Rao K. Spectrum of water vapor in the 1.9 and 2.7 μ regions. J Mol Spectrosc 1973;47:403–8.
[7] Camy-Peyret C, Flaud JM, Guelachvili G, Amiot C. High resolution Fourier transform spectrum of water between 2930 and 4255 cm^{-1}. Mol Phys 1973;26:825–55.
[8] Camy-Peyret C, Flaud JM. The $3v_2$ band of $H_2^{16}O$. Spectrochim Acta A 1973;29:1711–5.
[9] Flaud JM, Camy-Peyret C, Maillard JP. Higher ro-vibrational levels of H_2O deduced from high resolution oxygen-hydrogen flame spectra between 2800 and 6200 cm^{-1}. Mol Phys 1976;32:499–521.
[10] Flaud JM, Camy-Peyret C, Maillard JP. The H_2O spectrum between 4200 and 5000 cm^{-1}. J Mol Spectrosc 1977;65:219–28.
[11] Camy-Peyret C, Flaud JM, Toth RA. Vibration-rotation intensities for the $3v_2$, v_1+v_2, and v_2+v_3 bands of $H_2^{16}O$. J Mol Spectrosc 1977;67:117–31.
[12] Toth RA, Camy-Peyret C, Flaud JM. Strengths of H_2O lines in the 5000–5750 cm^{-1} region. JQSRT 1977;18:515–23.
[13] Flaud JM, Camy-Peyret C, Maillard JP, Guelachvili G. Higher ro-vibrational levels of H_2O deduced from high resolution oxygen-hydrogen flame spectra between 6200 and 9100 cm^{-1}. Mol Phys 1977;33:1641–50.
[14] Camy-Peyret C, Flaud JM, Maillard JP. The $4v_2$ band of $H_2^{16}O$. J Phys 1980;41:L23–6.
[15] Toth RA. $2v_2–v_2$ and $2v_2$ bands of $H_2^{16}O$, $H_2^{17}O$, and $H_2^{18}O$: line positions and strengths. J Opt Soc Am B 1993;10:1526–44.
[16] Toth RA. $v_1–v_2$, $v_3–v_2$, v_1, and v_3 bands of $H_2^{16}O$: line positions and strengths. J Opt Soc Am B 1993;10:2006–29.
[17] Toth RA. Extensive measurements of $H_2^{16}O$ line frequencies and strengths: 5750–7965 cm^{-1}. Appl Opt 1994;33:4851–67.
[18] Mikhailenko SN, Tyuterev VLG, Keppler KA, Winnewisser BP, Winnewisser M, Mellau G, et al. The $2v_2$ band of water: analysis of new FTS measurements and high-K_a transitions and energy levels. J Mol Spectrosc 1997;184:330–49.
[19] Mikhailenko SN, Tyuterev VLG, Starikov VI, Albert KK, Winnewisser BP, Winnewisser M, et al. Water spectra in the 4200–6250 cm^{-1} region: extended analysis of v_1+v_2, v_2+v_3, and $3v_2$ bands and confirmation of highly excited states from flame spectra and from atmospheric long-path observations. J Mol Spectrosc 2002;213:91–121.
[20] Smith KM, Ptashnik I, Newnham DA, Shine KP. Absorption by water vapour in the 1–2 μm region. JQSRT 2004;83:735–49.
[21] Macko P, Romanini D, Mikhailenko SN, Naumenko OV, Kassi S, Jenouvrier A, et al. High sensitivity CW-cavity ring down spectroscopy of water in the region of the 1.5 μm atmospheric window. J Mol Spectrosc 2004;227:90–108.
[22] Toth RA. Measurements of positions, strengths and self-broadened widths of H_2O from 2900 to 8000 cm^{-1}: line strength analysis of the second triad bands. JQSRT 2005;94:51–107.
[23] Toth RA, Flaud JM, Camy-Peyret C. Spectrum of $H_2^{18}O$ and $H_2^{17}O$ in the 5030–5640 cm^{-1} region. J Mol Spectrosc 1977;67: 185–205.
[24] Camy-Peyret C, Flaud JM, Mandin JY, Toth RA. Line positions and intensities for the v_1+v_2 and v_2+v_3 bands of $H_2^{18}O$. J Mol Spectrosc 1978;70:361–73.
[25] Chevillard JP, Mandin JY, Flaud JM, Camy-Peyret C. $H_2^{18}O$: The (0 3 0), (1 1 0), and (0 1 1) interacting states. Line positions and intensities for the $3v_2$, v_1+v_2, and v_2+v_3 bands. Can J Phys 1985;63:1112–27.
[26] Chevillard JP, Mandin JY, Camy-Peyret C, Flaud JM. The $2v_2+v_3–v_2$ hot band of $H_2^{18}O$ between 4800 and 6000 cm^{-1}: line positions and intensities. JQSRT 1986;36:395–8.
[27] Chevillard JP, Mandin JY, Camy-Peyret C, Flaud JM. The first hexad [(0 4 0), (1 2 0), (0 2 1), (2 0 0), (1 0 1), (0 0 2)] of $H_2^{18}O$: experimental energy levels and line intensities. Can J Phys 1986;64:746–61.
[28] Toth RA. The ν_1 and ν_3 bands of $H_2^{17}O$ and $H_2^{18}O$: line positions and strengths. J Mol Spectrosc 1994;166:184–203.
[29] Bykov AD, Zotov OV, Kamalov MR, Makarov VS, Naumenko OV. Analysis of the v_2+v_3 absorption band of the molecule of $H_2^{17}O$. Atmos Ocean Opt 1990;3:647–50.
[30] Toth RA, Brault JW. Line positions and strengths in the (0 1 1), (1 1 0), and (0 3 0) bands of HDO. Appl Opt 1983;22:908–26.
[31] Toth RA. Line positions and strengths of HDO between 6000 and 7700 cm^{-1}. J Mol Spectrosc 1997;186:66–89.
[32] Toth RA. Measurements of HDO between 4719 and 5843 cm^{-1}. J Mol Spectrosc 1997;186:276–92.
[33] Ulenikov ON, Hu SM, Bekhtereva ES, Onopenko GA, Wang XH, He SG, et al. High-resolution Fourier transform spectrum of HDO in the region 6140–7040 cm^{-1}. J Mol Spectrosc 2001;208:224–35.
[34] Toth RA. Measurements and analysis (using empirical functions for widths) of air- and self-broadening parameters of H_2O. JQSRT 2005;94:1–50.
[35] Rothman LS, Jacquemart D, Barbe A, Benner DC, Birk M, Brown LR, et al. The HITRAN 2004 molecular spectroscopic database. JQSRT 2005;96:139–204.
[36] Rothman LS, Barbe A, Benner DC, Brown LR, Camy-Peyret C, Carleer MR, et al. The HITRAN molecular spectroscopy database: edition of 2000 including updates trough 2001. JQSRT 2003;82:5–44.
[37] Carleer M, Jenouvrier A, Vandaele AC, Bernath PF, Merienne MF, Colin R, et al. The near infrared, visible and near ultraviolet overtone spectrum of water. J Chem Phys 1999;111:2444–50.
[38] Coheur PF, Fally S, Vandaele AC, Hermans C, Jenouvrier A, Carleer M, et al. Absolute intensities of water vapor lines in the near ultraviolet and visible regions. SPIE Proc Ser 2001;4168:97–105.
[39] Lundsberg-Nielsen L, Hegelund F, Nicolaisen FM. Analysis of the high resolution spectrum of ammonia ($^{14}NH_3$) in the near-infrared region, 6400–6900 cm^{-1}. J Mol Spectrosc 1993;162:230–45.
[40] Carleer M. Wspectra: a Windows program to measure accurately the line intensities of high resolution Fourier transform spectra. SPIE Proc Ser 2001;4168:337–42.
[41] Vander Auwera J. Absolute intensities measurements in the v_4+v_5 bands of $^{12}C_2H_2$: analysis of Herman–Wallis effects and forbidden transitions. J Mol Spectrosc 2000;201:143–50.
[42] Plateaux JJ, Regalia L, Boussin C, Barbe A. Multispectrum fitting technique for data recorded by Fourier transform spectrometer: application to N_2O and CH_3D. JQSRT 2001;68:507–20.

[43] Toth RA, Brown LR, Plymate C. Self broadened widths and frequency shifts of water vapor lines between 590 and 2400 cm^{-1}. JQSRT 1998;59:529–62.
[44] Grossmann BE, Browell EV. Spectroscopy of water vapor in the 720-nm wavelength region: line strengths, self-induced pressure broadenings and shifts, and temperature dependence of linewidths and shifts. J Mol Spectrosc 1989;136:264–94.
[45] Partridge H, Schwenke DW. The determination of an accurate isotope dependent potential energy surface for water from extensive *ab initio* calculations and experimental data. J Chem Phys 1997;106:4618–39.
[46] Schwenke DW, Partridge H. Convergence testing of the analytic representation of an *ab initio* dipole moment function for water: improved fitting yields improved intensities. J Chem Phys 2000;113:6592–7.
[47] Tashkun SA, Perevalov VI, Teffo JL, Bykov AD, Lavrentieva NN. CDSD-1000, the high temperature carbon dioxide spectroscopic databank. JQSRT 2003;82:165–96.
[48] Mikhailenko SN, Tyuterev VLG, Mellau G. (0 0 0) and (0 1 0) states of $H_2^{18}O$: analysis of rotational transitions in hot emission spectrum in the 400–850 cm^{-1} region. J Mol Spectrosc 2003;217:195–211.
[49] Tennyson J, Zobov NF, Williamson R, Polyansky OL, Bernath PF. Experimental energy levels of the water molecule. J Phys Chem Ref Data 2001;30:735–831.
[50] Coudert LH, Pirali O, Vervloet M, Lanquetin R, Camy-Peyret C. The eight first vibrational states of the water molecule: measurements and analysis. J Mol Spectrosc 2004;228:471–98.
[51] Mikhailenko SN, Tyuterev VLG, Brault JW. Private communication, 2001.
[52] Toth RA. Transition frequencies and strengths of $H_2^{17}O$ and $H_2^{18}O$: 6600 to 7640 cm^{-1}. Appl Opt 1994;33:4868–79.
[53] Toth RA. Water vapor measurements between 590 and 2582 cm^{-1}: line positions and strengths. J Mol Spectrosc 1998;190:379–96.
[54] Flaud JM, Camy-Peyret C. The interacting states (0 2 0), (1 0 0), and (0 0 1) of $H_2^{16}O$. J Mol Spectrosc 1974;51:142–50.
[55] Tyuterev VLG. The generating function approach to the formulation of the effective rotational Hamiltonian: a simple closed form model describing strong centrifugal distortion in water-type nonrigid molecules. J Mol Spectrosc 1992;151:97–129.
[56] Starikov VI, Tashkun SA, Tyuterev VLG. Description of vibration–rotation energies of nonrigid triatomic molecules using the generating function method. Bending states and second triad of water. J Mol Spectrosc 1992;151:130–47.
[57] Parekunnel T, Bernath PF, Zobov NF, Shirin SV, Polyansky OL, Tennyson J. Emission spectrum of hot HDO in the 380–2190 cm^{-1} region. J Mol Spectrosc 2001;210:28–40.
[58] Bykov AD, Voronin BA, Naumenko OV, Petrova TM, Sinitsa LN. Spectroscopic constants of the (0 1 1), (2 0 0), (1 2 0) and (0 4 0) states of the $HD^{16}O$ molecule. Atmos Ocean Opt 1999;12:786–91.
[59] Jacquinet-Husson N, Scott NS, Chedein A, Garceran K, Armante R, Chursin AA, et al. The 2003 edition of the GEISA/IASI spectroscopic database. JQSRT 2005;95:429–67.
[60] Mikhailenko SN, Albert KK, Mellau G, Klee S, Winnewisser M, Winnewisser B, et al. Water intensity measurement in the Giessen spectra revisited: 1900–6600 cm^{-1} region. JQSRT 2006, submitted for publication.
[61] Ptashnik IV, Smith KM, Shine KP. Self-broadened line parameters for water vapour in the spectral region 5000–5600 cm^{-1}. J Mol Spectrosc 2005;232:186–201.
[62] Tashkun SA, Schwenke DW, Tyuterev VLG. Nineteenth Colloquium on High Resolution Molecular Spectroscopy, Salamanca, Spain, September, 2005.
[63] Gamache RR, Hartmann JM. An intercomparison of measured pressure-broadening and pressure-shifting parameters of water vapor. Can J Chem 2004;82:1013–27.
[64] Brown LR, Toth RA, Dulick M. Empirical line parameters of $H_2^{16}O$ near 0.94 μm: positions, intensities and air-broadening coefficients. J Mol Spectrosc 2002;212:54–82.
[65] Gamache RR, Fischer J. Half-widths of $H_2^{16}O$, $H_2^{18}O$, $H_2^{17}O$, $HD^{16}O$ and $D_2^{16}O$: I. Comparison between isotopomers. JQSRT 2003;78:289–304.
[66] Jacquemart D, Gamache R, Rothman LS. Semi-empirical calculation of air-broadened half-widths and air pressure-induced frequency shifts of water-vapor absorption lines. JQSRT 2005;96:205–39.